polymers

MDPI

Article

Synthesis of Comb-like and Coil-Comb Polystyrene–Polyglycidol Copolymers via Click Chemistry: Self-Assembly and Biological Evaluation

Natalia Toncheva-Moncheva [1,2,*], Erik Dimitrov [1,2], Niya Delcheva [1], Denitsa Momekova [3], Magdalena Kondeva-Burdina [4], Denitsa Stefanova [4], Virginia Tzankova [4], Stergios Pispas [5] and Stanislav Rangelov [1,2]

1 Institute of Polymers, Bulgarian Academy of Sciences, Akad. G. Bonchev St. 103A, 1113 Sofia, Bulgaria; e_dimitrov@polymer.bas.bg (E.D.); n_delcheva@polymer.bas.bg (N.D.); rangelov@polymer.bas.bg (S.R.)
2 Centre of Competence "Sustainable Utilization of Bio-resources and Waste of Medicinal and Aromatic Plants for Innovative Bioactive Products" (BIORESOURCES BG), 1000 Sofia, Bulgaria
3 Department of Pharmaceutical Technology and Biopharmaceutics, Faculty of Pharmacy, Medical University of Sofia, 2 Dunav Street, 1000 Sofia, Bulgaria; dmomekova@pharmfac.mu-sofia.bg
4 Department of Pharmacology, Pharmacotherapy and Toxicology, Faculty of Pharmacy, Medical University of Sofia, 2 Dunav Street, 1000 Sofia, Bulgaria; mkondeva@pharmfac.mu-sofia.bg (M.K.-B.); denitsa.stefanova@pharmfac.mu-sofia.bg (D.S.); vtzankova@pharmfac.mu-sofia.bg (V.T.)
5 Theoretical and Physical Chemistry Institute, National Hellenic Research Foundation, 48 Vass. Constantinou Avenue., 116 35 Athens, Greece; pispas@eie.gr
* Correspondence: ntoncheva@polymer.bas.bg

Abstract

Amphiphilic copolymers based on polystyrene and polyglycidol combine the chemical inertness of polystyrene with the biocompatibility of polyglycidol, making them attractive materials for polymeric micelles. While comb-like architectures have been explored to control micellization behavior and biological response, a direct comparison between comb-like and coil-comb topologies in polystyrene–polyglycidol copolymers at identical polyglycidol content remains insufficiently investigated. In this work, amphiphilic comb-like and coil-comb polystyrene–polyglycidol copolymers were synthesized via copper-catalyzed azide–alkyne click chemistry by grafting a monoalkyne-terminated polyglycidol precursor onto azide-functionalized random and block styrene copolymers. The copolymers were characterized by size exclusion chromatography and nuclear magnetic resonance. Polymeric micelles were prepared by nanoprecipitation, and their self-assembly in aqueous solution was investigated by critical micelle concentration determination, dynamic and electrophoretic light scattering, and atomic force microscopy. Both copolymers formed stable aqueous dispersions and exhibited comparable critical micelle concentrations. At identical polyglycidol content, the random copolymer formed a uniform, monomodal micellar population, whereas the block-based coil-comb architecture led to bimodal size distributions, indicating the coexistence of two distinct micellar populations. The investigated systems showed low cytotoxicity and did not induce significant oxidative stress within the studied concentration range. On isolated rat brain sub-cellular fractions (synaptosomes, mitochondria and microsomes), administered alone, the comb-like and coil-comb polystyrene-polyglycidol copolymers did not reveal statistically significant neurotoxic effects. The results demonstrate that macromolecular architecture plays a key role in governing micellar organization and in vitro biological response in polystyrene–polyglycidol copolymers, highlighting their potential as architecture-controlled polymer-based nanocarriers.

Academic Editor: Ivan Gitsov

Received: 3 January 2026
Revised: 4 February 2026
Accepted: 9 February 2026
Published: 19 February 2026

Keywords: linear polyglycidol; comb-like and coil-comb chain architecture; click chemistry; self-assembly; polymer micelles; nanoparticles; light scattering; nanocarriers

1. Introduction

Nowadays, the advancement of polymer nanotechnology has opened up opportunities to develop controlled delivery nanodevices for drugs and small molecules, which has resulted in a number of benefits [1–3] such as time-controlled and site-specific delivery, prolonged blood circulation of active therapeutics, and prioritized accumulation at tumor sites owing to the enhanced permeability and retention (EPR) effect, while minimizing undesirable side effects [4]. Collectively, these advantages yield more favorable pharmacokinetic profiles and allow researchers to evaluate applications of polymeric nanomaterials in a wide range of clinical problems, with the goal of developing improved and more efficient therapeutics [5].

Among the various types of drug delivery systems (DDS) and considering the rapid development of methods for synthetic elaboration of macromolecular architectures, polymeric micelles are the most widely studied systems in the chemical realm, which involves the integration of multiple functionalities, targeting ligands, and the development of methods to control their shape, loading capacity, and dispersity [5]. Polymeric micelles represent three-dimensional structures made by self-assembly of amphiphilic macromolecules at polymer concentrations above the critical micelle concentration (CMC). Typically, they are characterized by small particle size, narrow size distribution, slow rate of dissociation, and the ability to avoid the rapid uptake by the reticuloendothelial system (RES). The small size, typically in the range of tens to several hundreds of nanometers in diameter, enables cell entry via endocytosis [5,6].

The frequently utilized amphiphilic macromolecules are composed of preferably biodegradable, biocompatible, or chemically inert segments: the hydrophobic segments form the micellar core, while the hydrophilic ones surround the core, thus stabilizing the nanostructure. The commonly used hydrophobic core constituents are polymers based on poly(lactic acid), poly(lactic-co-glycolic acid), poly(propylene oxide) (PPO), poly(ε-caprolactone), and polystyrene (PS), while hydrophilic polymers such as poly(ethylene glycol) (PEG), chitosan, poly(acrylic acid), hyaluronic acid, poly(2-oxazolines) and polyvinylpyrrolidone form the shell [7–13]. Typically, the polymers are prepared as linear di-, triblock and rarely of non-linear chain architectures, which greatly influences their chain conformation and self-assembly behavior. Among the various nonlinear chain topologies, the comb-like architecture is unique, resulting in interesting morphological properties of the obtained micelles [14,15]. In particular, it is interesting to design amphiphilic comb-like copolymers, the side chains of which are arranged on the homopolymer, block or random copolymer main chain [16], as such architectures provide opportunities to tailor the molecular topology and composition, and also the morphology of the formed micelles, allowing precise control over their hydrophilic–hydrophobic balance, size, stability, and drug-loading capacity. The structural and morphological features of comb-like architectures contribute to favorable biological performance, including enhanced micellar stability in physiological media and nanoscale characteristics relevant to cellular uptake and biocompatibility. The diversity of amphiphilic copolymer systems comprising coil-comb chain architecture can be developed on the basis of polystyrene due to its facile synthesis and the possibility to attach functional moieties, thereby linking different hydrophilic blocks to the polystyrene chains [8,13,17–19].

Beyond its synthetic versatility, the hydrophobic and biologically inert nature of polystyrene allows the encapsulation of hydrophobic or water-insoluble drugs, enhances drug stability, and thereby increases their bioavailability under physiological conditions. Moreover, due to the glassy nature of polystyrene at ambient and physiological temperatures, amphiphilic copolymers containing PS segments often exhibit reduced chain mobility within micellar cores, which can result in kinetically stabilized micellar assemblies in biologically relevant aqueous environments [20,21].

Traditionally, polystyrene-based systems with improved biocompatibility can be obtained by introducing PEG, and a variety of such systems have been described in the literature [22–24]. Although PEG is one of the most widely used hydrophilic polymers in drug delivery systems and is approved by the Food and Drug Administration (FDA), its application has recently been questioned due to several drawbacks, including the induction of anti-PEG antibodies, hypersensitivity reactions, limited functionalization, and non-biodegradability, leading to potential accumulation in vivo [25–27].

A promising alternative to PEG—its linear polyether analog, polyglycidol (PG)—is rapidly emerging. PG, also known as polyglycerol, has been extensively studied because its chain structure is similar to PEG and its physicochemical properties can be tailored through appropriate protection and deprotection strategies during polymer synthesis. It exhibits high biocompatibility, chemical stability, and additional advantages over PEG, such as ease of synthesis, controllable structure, oxidation resistance, and multiple hydroxyl functionality [28–30]. These functional groups allow further modification and covalent attachment of small molecules to PG chains, thereby improving the therapeutic performance of the obtained PG based micellar carriers and expanding their potential biomedical and pharmaceutical applications. Generally, linear PG can be obtained via ring-opening anionic polymerization of protected glycidyl ethers, followed by deprotection [31].

Polystyrene–polyglycidol (PS–PG) copolymers have been reported as amphiphilic materials combining the inherent hydrophobicity and rigidity of polystyrene with the hydrophilicity and multifunctionality of the polyglycidol. Early studies demonstrated the feasibility of PS–PG block copolymer synthesis and their self-assembly in selective solvents [32], while recent investigations emphasized the multifunctional hydroxyl-rich nature of PG segments, enabling versatile post-modification and bioconjugation [33]. Subsequent works confirmed that PS–PG systems form well-defined micellar aggregates in aqueous media and exhibit tunable hydrophilicity and surface properties [13,34]. Such copolymers—primarily in block or graft architectures—are therefore considered promising amphiphilic materials for biomedical applications [35]. However, studies exploring PS–PG copolymers with well-defined comb, coil–comb, or brush–coil–brush topologies remain limited [34,36], which motivates the present investigation.

The objective of this work is to synthesize amphiphilic comb-like and coil-comb copolymers comprising PG side chains distributed along the copolymer backbone in distinct distribution patterns. To achieve these goals, we applied a *click* chemistry approach in which monoalkyne-functionalized PG precursor, poly(ethoxyethyl glycidyl ether (PEEGE), was conjugated to azide-modified poly(styrene-*ran*-4-chloromethylstyrene) and polystyrene-*block*-poly(4-chloromethylstyrene) copolymers. Further, the aqueous solution properties of the resulting copolymers, particularly the formation of well-defined nanosized micellar aggregates and the evaluation of their potential as drug delivery vehicles, are presented and discussed in detail. In addition, the study aims to thoroughly evaluate the biocompatibility of the newly synthesized copolymers using several in vitro cell models that represent different potential routes of administration for the resulting drug-delivery nanoplatforms prepared thereof.

2. Materials and Methods

2.1. Materials

1-phenyl-1-(2,2,6,6-tetramethyl-1-piperidinyloxy)ethane (>98%, Sigma-Aldrich, St. Louis, MO, USA), p-chloromethylstyrene (CMS, >90% Sigma-Aldrich, St. Louis, MO, USA), acetic anhydride (Ac_2O, ReagentPlus®, ≥99%, Sigma-Aldrich, St. Louis, MO, USA), styrene (stabilized for synthesis Sigma-Aldrich, St. Louis, MO, USA), 4-(chloromethyl)styrene (CMS > 90%, Sigma-Aldrich, St. Louis, MO, USA), sodium azide (ReagentPlus®, ≥99.5%, Sigma-Aldrich, St. Louis, MO, USA), magnesium sulfate (anhydrous, ReagentPlus®, ≥99.5%, Sigma-Aldrich, St. Louis, MO, USA), glycidol (2,3-epoxypropanol, 96%, Aldrich, St. Louis, MO, USA), ethyl vinyl ether (99%, Aldrich, St. Louis, MO, USA), p-toluenesulfonic acid (ACS reagent, ≥98.5%, Sigma-Aldrich, St. Louis, MO, USA), sodium sulfate (≥99.99% trace metals basis, anhydrous, Sigma-Aldrich, St. Louis, MO, USA), sodium hydrogen carbonate (anhydrous, ≥99.7%, Sigma-Aldrich, St. Louis, MO, USA), potassium (cubes in mineral oil, 99.5% trace metals basis, Sigma-Aldrich, St. Louis, MO, USA), tert-butanol (anhydrous ≥ 99.5%, Sigma-Aldrich, St. Louis, MO, USA), 4-pentynoic acid (95%, Acros Organics, Geel, Belgium), 4-(dimethylamino)pyridine (DMAP, ReagentPlus®, ≥99%, Sigma-Aldrich, St. Louis, MO, USA), *N*-(3-dimethylaminopropyl)-*N*′-ethylcarbodiimide hydrochloride (EDC, commercial grade, powder, Sigma-Aldrich, St. Louis, MO, USA), *N*,*N*,*N*′,*N*″,*N*‴-pentamethyldiethylenetriamine (PMDETA, 99%, Sigma-Aldrich, St. Louis, MO, USA), copper(I) bromide (99.999% trace metals basis, Sigma-Aldrich, St. Louis, MO, USA) and $AlCl_3 \cdot 6H_2O$ (99%, Sigma-Aldrich, St. Louis, MO, USA) were used as received. Propylene oxide (PO, 99%, Sigma-Aldrich, St. Louis, MO, USA) was dried over CaH_2, distilled, and stored over a 4 Å molecular sieve before use. *N*,*N*-dimethylformamide (DMF, ACS reagent, ≥99.8%, Sigma-Aldrich, St. Louis, MO, USA) and dimethyl sulfoxide (DMSO, ≥99.9%, ACS reagent, Sigma-Aldrich, St. Louis, MO, USA) were dried by molecular sieves. Methylene chloride (>99.98%, Fisher Scientific, Waltham, MA, USA) and tetrahydrofuran (>99.5%, Fisher Scientific, Waltham, MA, USA) were dried using calcium hydride and freshly distilled before use. Cyclohexane (Aldrich, 99.8%, St. Louis, MO, USA), chloroform (Sigma-Aldrich, 99%, St. Louis, MO, USA) and methanol (Merck, 99.8%, Darmstadt, Germany) were used as received. Deionized water was obtained by Millipore MilliQ system (Millipore, Burlington, MA, USA) and was additionally filtered through a 220 nm PTFE filter and a 20 nm cellulose filter.

2.2. Cell Lines

The in vitro effects of the synthesized copolymers on cell viability and proliferation were assessed across several cell lines: HL-60 cells (the acute myeloid leukemia) were obtained from the German Collection of Microorganisms and Cell Cultures (DSMZ GmbH, Braunschweig, Germany). The L929 (mouse fibroblast-like cell line), Ea.hy926 (human umbilical vein endothelial cell hybrid line), and SH-SY5Y (human neuroblastoma) cell lines were acquired from the European Collection of Authenticated Cell Cultures (ECACC, Salisbury, UK). L929 and Ea.hy926 cells were maintained in Dulbecco's Modified Eagle Medium (DMEM) containing 10% fetal bovine serum (FBS) and a conventional antibiotic supplement: (100 U/mL penicillin and 100 µg/mL streptomycin; Devon, UK), and SH-SY5Y were grown in Roswell Park Memorial Institute (RPMI) 1640 medium supplemented with 10% heat-inactivated FBS, 2 mM L-glutamine, and 1% (*v*/*v*) penicillin–streptomycin solution to prevent microbial contamination. HL-60 cells were maintained in RPMI-1640 medium supplemented with 10% fetal bovine serum. Cultures were incubated at 37 °C in humidified conditions with 5% CO_2 using BB 16-Function Line incubators (Heraeus, Kendro, Hanau, Germany).

2.3. Animals

Six Wistar rats (200–250 g body weight) were included in the study. The animals were sourced from the National Breeding Center of the Bulgarian Academy of Sciences (Sofia, Bulgaria) and housed in Plexiglas cages under standard laboratory conditions, with ad libitum access to food and water and a 12 h light/dark cycle at 20–25 °C. Twelve hours before each specific study, the animals' food was withdrawn. The experiments were conducted in accordance with the Ordinance No. 15 on Minimum Requirements for the Protection and Welfare of Experimental Animals (SG No. 17, 2006) and the European Regulation for the Handling of Experimental Animals, and under Permission No. 304, valid until 28 June 2026, issued by the Bulgarian Food Safety Agency. The detailed procedure used for animal euthanasia and subsequent brain tissue processing was as follows. Animals were euthanized by decapitation using a special guillotine designed for laboratory rats, without the use of chemical anesthetics. The brain was isolated by opening the skull. The isolated brain was homogenized, and brain subcellular fractions were obtained according to the relevant protocol:

- synaptosomes and brain mitochondria are obtained using a Percoll gradient;
- brain microsomes are obtained by double centrifugation.

2.4. Synthesis of Comb-like and Coil-Comb Conjugates Comprising Polymer Main Chains of Poly(Styrene-ran-Azidomethylstyrene) P(S-ran-N_3MS) or Polystyrene-Block-Poly(AZIDOMETHYLSTYRENE) (PS-Block-PN_3MS) and Polyglycidol Pendant Side Chains

2.4.1. Synthesis and Azide Functionalization of Poly(4-Chloromethylstyrene) Copolymers

Poly(styrene-*ran*-4-chloromethylstyrene) random copolymer [P(S-*ran*-CMS)] and polystyrene-*block*-poly(4-chloromethylstyrene) block copolymer [PS-*block*-PCMS] were synthesized by nitroxide-mediated controlled radical polymerization, as previously reported [37–39]. Their molar mass characteristics and composition, determined by SEC, are summarized in Table S1. The conversion of chloromethyl groups into azide functionalities was verified by ^{1}H NMR and SEC (Supplementary Materials, Scheme S1 and Figures S1 and S2).

2.4.2. Synthesis of Monoalkyne-Terminated Poly(Ethoxyethyl Glycidyl Ether) (PEEGE)

Monoalkyne-terminated PEEGE was synthesized by ring-opening anionic polymerization of ethoxyethyl glycidyl ether (EEGE) [7,28] and functionalized via introduction of an alkyne end group. The obtained polymer was characterized by SEC, ^{1}H NMR, and IR spectroscopy, and the reaction pathway is presented in Supplementary Materials (Scheme S2 and Figures S3–S5). The polymer composition was determined by ^{1}H NMR analysis based on signal integration, as shown in Supplementary Materials (Figure S6).

2.4.3. Cleavage of the Protective Ethoxyethyl Groups

The deprotection procedure is based on the method developed by Namboodiri [40] and modified by Dimitrov et al. [41], using the Lewis acid $AlCl_3.6H_2O$. A detailed description is provided in Supplementary Materials (Figure S6).

2.4.4. Synthesis of Amphiphilic Copolymers Comprising a Comb-like Chain Architecture Using an Azide-Alkyne Click Chemistry Approach

Monoalkyne-terminated PEEGE (186.7 mg, 46.675 µmol, 5 eq) was dissolved in 7.5 mL of dry THF and placed in a 50 mL round-bottom flask under an argon atmosphere. The solution was purged with argon and stirred vigorously for 20 min. Separately, P(S-*ran*-N_3MS) random copolymer (93.35 mg, 9.335 µmol, 1 eq) was dried by azeotropic distillation in toluene. The dry product was dissolved in 7.5 mL of dry THF and added

via syringe to the PEEGE solution. Copper (I) bromide (66.9 mg, 0.466 mmol, 10 equiv. per alkyne group) and PMDETA (80.8 mg, 0.466 mmol, 10 equiv. per alkyne group) were used as a catalyst. The azide-alkyne *click* coupling reaction was carried out under argon at 30 °C for 24 h. The reaction mixture was cooled to room temperature, and the product was purified by column chromatography using neutral Al_2O_3 as the stationary phase, with THF as eluent. The obtained conjugate is referred to as [P(S-*ran*-CMS)]-*graft*-PEEGE. Yield: 214.19 mg, 77%. ^{1}H NMR (600 MHz, $CDCl_3$) δ 7.55–7.32 (H from triazole ring) 7.23–6.25 (Ar H), 5.06–4.85 (-C$\underline{H_2}$-N), 4.36–4.00 (-C$\underline{H}$(CH_3)-O-CH_2-CH_3), 4.00–3.20 (-O-$\underline{CH_2}$-C$\underline{H}$($\underline{CH_2}$-O-)-O- and -C$\underline{H}$(CH_3)-O-C$\underline{H_2}$-CH_3), 2.00–1.23 (-CH_2-C$\underline{H}$< and -CH($\underline{CH_3}$)-O-CH_2-C$\underline{H_3}$,), SEC: Mn = 41,220 g/mol, Mw = 45,540 g/mol, $Đ$ = 1.10.

The cleavage of the ethoxyethyl protecting groups of glycidol was performed by following the procedure described above. In brief, the polymers were dissolved in 20 mL of methanol, and a catalytic amount of $AlCl_3.6H_2O$ (20 mg) was added. The reactions were carried out at 40 °C for 48 h. The aluminum salt was purified by column chromatography using diatomaceous earth as an adsorbent. The obtained conjugate is denoted [P(S-*ran*-CMS)]-*graft*-PG: Yield: 133.12 mg, 97.1%, ^{1}H NMR (600 MHz, DMSO-d_6) δ 7.94–7.74 (triazole H) 7.27–6.21 (Ar H), 5.50–5.30 (-C$\underline{H_2}$-N), 4.62–4.49 (-CH_2O$\underline{H}$), 3.62–3.27 (-O-$\underline{CH_2}$-C$\underline{H}$($\underline{CH_2}$-O-)-O-), 2.00–1.23 (-CH_2-C$\underline{H}$<).

2.4.5. Synthesis of Amphiphilic Copolymers Comprising Coil-Comb Chain Architecture Using an Azide-Alkyne Click Chemistry Approach

Monoalkyne-terminated PEEGE (192.4 mg, 48.1000 μmol, 7 eq) was dissolved in 7.5 mL of dry THF and placed in a round-bottom flask under argon atmosphere. The solution was purged with argon and stirred vigorously for 20 min. Separately, PS-*block*-PN_3MS block copolymer (101.81 mg, 6.17 μmol, 1 eq) was dried by azeotropic distillation in toluene. The dry product was dissolved in 7.5 mL of dry THF and added via syringe to the alkyne-terminated PEEGE solution. Copper (I) bromide (70.68 mg, 0.493 mmol, 10 equiv. per alkyne group) and PMDETA (64.1 mg, 0.372 mmol, 10 equiv. per alkyne group) were used as the catalyst. The azide-alkyne *click* coupling reaction was carried out under argon at 30 °C for 24 h. The reaction mixture was cooled to room temperature and purified following the procedure described above. The obtained conjugate is denoted [PS-*block*-PCMS]-*graft*-PEEGE. Yield: 253 mg, 85%. ^{1}H NMR (600 MHz, $CDCl_3$) δ 7.55–7.32 (triazole ring H) 7.23–6.25 (Ar H), 5.06–4.85 (-C$\underline{H_2}$-N), 4.36–4.00 (-C$\underline{H}$(CH_3)-O-CH_2-CH_3), 4.00–3.20 (-O-$\underline{CH_2}$-C$\underline{H}$($\underline{CH_2}$-O-)-O- and -C$\underline{H}$(CH_3)-O-C$\underline{H_2}$-CH_3), 2.00–1.23 (-CH_2-C$\underline{H}$< and -CH($\underline{CH_3}$)-O-CH_2-C$\underline{H_3}$),: Mn = 27,670 g/mol, Mw = 38,800 g/mol, $Đ$ = 1.40.

The cleavage of the ethoxyethyl protecting groups of glycidol was performed by following the procedure described above. The obtained conjugate is denoted [PS-*block*-PCMS]-*graft*-PG: Yield: 159.17 mg, 98.3%. ^{1}H NMR (600 MHz, DMSO-d_6) δ 7.94–7.74 (H from triazole ring) 7.27–6.21 (Ar H), 5.50–5.30 (-C$\underline{H_2}$-N), 4.62–4.49 (-CH_2O$\underline{H}$), 3.62–3.27 (-O-$\underline{CH_2}$-C$\underline{H}$($\underline{CH_2}$-O-)-O-), 2.00–1.23 (-CH_2-C$\underline{H}$<).

Based on the molar feed ratios of monoalkyne-terminated PEEGE to the azide-functionalized polymer backbones, the target grafting densities ($N_{graft,theor}$) were estimated (see Section V in Supplementary Materials). For the random copolymer [P(S-*ran*-CMS)]-*graft*-PEEGE, the feed ratio corresponded to approximately five grafts per chain, whereas for the block copolymer [PS-*block*-PN_3MS]-*graft*-PEEGE, the theoretical value was about eight grafts per chain. These target values served as references for subsequent structural characterization and for comparison with experimental data derived from ^{1}H NMR analyses.

2.5. Methods

2.5.1. Size Exclusion Chromatography (SEC)

Analyses were performed on a Shimadzu Nexera HPLC chromatograph (Shimadzu Corporation, Kyoto, Japan), equipped with a degasser, a pump, an auto-sampler, an RI detector and three columns: 10 μm PL gel mixed-B, 5 μm PL gel 500 Å and 50 Å. Tetrahydrofuran was used as the eluent at a flow rate of 1.0 mL.min^{-1} and a temperature of 40 °C. The sample concentration was 1 mg/mL, and SEC was calibrated with polystyrene standards.

2.5.2. Nuclear Magnetic Resonance (^{1}H NMR)

^{1}H NMR measurements were conducted on a Bruker Avance II spectrometer (Bruker BioSpin GmbH, Rheinstetten, Germany) operating at 600 MHz using $CDCl_3$, CD_3OD, or DMSO-d6 as the solvents at 25 °C.

2.5.3. Fourier-Transform Infrared Spectroscopy (FTIR)

FTIR spectra were measured with an attenuated total reflection (ATR) spectrophotometer (IRAffinity-1, Shimadzu, Kyoto, Japan) in the 450–4500 cm^{-1} range at a resolution of 1 cm^{-1}.

2.5.4. Spectrophotometric Determination of the Critical Micelle Concentration (CMC)

Here, 20 μL of a 0.4 mM solution of 1,6-diphenyl-1,3,5-hexatriene (DPH) in methanol was added to 2 mL of aqueous dispersions with increasing concentrations in the range 9.765×10^{-4}–1.0 mg/mL. The samples were incubated in the dark for 24 h at room temperature. UV–Vis absorption spectra of DPH in the wavelength range λ = 300–500 nm at room temperature were recorded on a Beckman Coulter DU 800 UV-VIS spectrophotometer. The intensities of the absorption peak at 356 nm were plotted against polymer concentration. The CMC value was determined as the break in the absorbance intensity versus concentration curve.

2.5.5. Atomic Force Microscopy (AFM)

The images were obtained using a Bruker Dimension Icon Instrument (Bruker, Santa Barbara, CA, USA) operating at a 1.00 Hz scan rate under ambient conditions. Further, 2 μL of the copolymer dispersions were placed onto a freshly cleaned glass substrate (1 cm^2) and spin-coated at 2000 rpm for a minute. AFM measurements were performed in ScanAsyst (Peak Force Tapping mode using MPP-11120-10 (RTESPA) AFM probes at (f_0 = 300 KHz, k = 40 N/m), Scan Rate 1 Hz). The cleaning procedure of the glass substrates used for AFM measurements is described in detail in the Supplementary Materials (Section VI).

2.5.6. Dynamic and Electrophoretic Light Scattering

The preliminary assessment of the particle size and size distribution was carried out by dynamic light scattering (DLS) measurements on a NanoBrook 90 Plus PALS instrument (Brookhaven Instruments Corporation, Holtsville, NY, USA), equipped with a 35 mW red diode laser (λ = 660 nm) at a scattering angle of 90°. The measurements were taken at 25 °C and 37 °C, applying a dust cut-off of 30 micellar dispersions at concentrations of 1 mg/mL and fixed volumes of 1.7 mL.

The apparent hydrodynamic radii (R_h^{90}) were determined according to the Stokes–Einstein equation:

$$R_h^{90} = kT/(6\pi\eta D_{90}) \quad (1)$$

where k is the Boltzmann constant, η is the solvent viscosity at temperature T in Kelvin, and D_{90} is the diffusion coefficient measured at an angle of 90°. Each measurement was performed in triplicate.

The electrophoretic light scattering measurements were carried out on the same instrument at a scattering angle of 15° and at 25 °C and 37 °C. The principle of phase analysis light scattering (PALS) was applied for the measurements of electrophoretic mobility. The ζ potentials were calculated using the Smoluchowski equation:

$$\zeta = 4\pi\eta\upsilon/\varepsilon \quad (2)$$

where η is the solvent viscosity, υ is the electrophoretic mobility, and ε is the dielectric constant of the solvent.

2.5.7. Cytotoxicity Assessment

Cell viability following exposure to different concentrations of the synthesized copolymers was assessed by the MTT colorimetric assay, following previously reported procedures [42,43]. Briefly, cells in the exponential growth phase were plated in 96-well flat-bottom plates at a density of 1×10^5 cells/mL (100 µL per well) and allowed to adhere for 24 h at 37 °C. The cultures were then treated with increasing concentrations of the test formulations and incubated for an additional 72 h. Upon completion of the treatment period, 300 µL of MTT solution (10 g/L in PBS) was added to each well, followed by incubation for 4 h at 37 °C. The resulting formazan crystals were solubilized using 100 µL per well of 2-propanol acidified with 5% formic acid. Absorbance was measured at 580 nm using a Labexim LMR-1 microplate reader. Cell viability was expressed as a percentage relative to untreated controls, and IC_{50} values were calculated from dose–response curves.

2.5.8. Preparation of Rat Brain Synaptosomes and Mitochondria

Synaptosomes and mitochondria were isolated through successive subcellular fractionation using a Percoll density gradient, as previously described [44]. Brain tissue was homogenized and initially centrifuged at 1000× *g* for 5 min at 4 °C. The resulting supernatant was collected and subjected to a second centrifugation under identical conditions. Supernatants from both spins were pooled and divided equally into four tubes. These samples were then centrifuged at 10,000× *g* for 20 min at 4 °C on three consecutive occasions, with the final two centrifugation steps serving to purify the synaptosomal and mitochondrial fractions.

2.5.9. Synaptosomes and Mitochondria Isolation

The isolation was performed with the help of a colloidal solution of silicon (Percoll). In brief, 1. A 90% stock solution of Percoll was prepared. 2. Percoll solutions of different percentages of 16% and 10% were prepared. We placed 4 mL each of 16% and 10% Percoll in six test tubes. 3. Following the final centrifugation step, Percoll was added to the precipitate to achieve a final concentration of 7.5% (from a 90% Percoll stock). The samples were then centrifuged at 15,000× *g* for 20 min at 4 °C. This procedure resulted in the formation of three distinct layers: a lower fraction enriched in mitochondria, an upper lipid-containing layer, and an intermediate band located at the 10–16% Percoll interface corresponding to synaptosomes. The appropriate fraction from each tube was carefully aspirated using a glass Pasteur pipette and pooled. Buffer B supplemented with glucose was subsequently added, and the suspension was centrifuged at 10,000× *g* for 20 min at 4 °C to replace the isolation medium with incubation buffer. After centrifugation, the resulting pellet—containing both synaptosomes and mitochondria—was resuspended in buffer B with glucose.

2.5.10. Evaluation of Synaptosomal Viability by MTT

Following 1 h of incubation, synaptosomes were centrifuged at 15,000× *g* for 1 min in a microcentrifuge. The resulting pellet was gently resuspended in buffer B containing glucose, while the supernatant was discarded, and the sample was subjected to a second centrifugation at 15,000× *g* for 1 min. After the second wash, the pellet was again resuspended in buffer B with glucose. To these washed synaptosomes, 60 µL of MTT solution was added, and the samples were incubated at 37 °C for 10 min. Post-incubation, the synaptosomes were centrifuged at 15,000× *g* for 2 min, the supernatant removed, and the resulting formazan crystals were dissolved in DMSO. The absorbance of the solubilized formazan was measured spectrophotometrically at 580 nm [45].

2.5.11. Reduced Glutathione (GSH) in Isolated Brain Synaptosomes

Reduced glutathione (GSH) in isolated brain synaptosomes was determined following protein precipitation with trichloroacetic acid. The thiol groups in the resulting supernatant were quantified using DTNB, producing a yellow-colored product with absorbance measured at 412 nm. After incubation, synaptosomes were centrifuged at 4000× *g* for 3 min, the supernatant discarded, and the pellet processed for GSH analysis. The pellet was treated with 5% trichloroacetic acid, incubated on ice for 10 min, and centrifuged at 8000× *g* for 10 min at 4 °C. The supernatant was collected for GSH measurement and stored at −20 °C. Immediately prior to analysis, samples were neutralized with 5 N NaOH [46].

2.5.12. Determination of Malondialdehyde (MDA) Production in Brain Mitochondria

To measure malondialdehyde (MDA) levels, 0.3 mL of 0.2% thiobarbituric acid and 0.25 mL of 0.05 M sulfuric acid were added to mitochondrial samples. The mixtures were then heated in a boiling water bath for 30 min. After cooling on ice, 0.4 mL of n-butanol was added to each tube, followed by centrifugation at 3500× *g* for 10 min. The concentration of MDA in the resulting supernatants was determined spectrophotometrically at 532 nm [47].

2.5.13. Determination of GSH Level in Brain Mitochondria

Following incubation, the mitochondrial reaction was terminated by the addition of 5% trichloroacetic acid. Each sample was homogenized in the acid and incubated on ice. The homogenates were then centrifuged at 6000× *g*, and 0.04% DTNB solution was added to the resulting supernatant, producing a yellow-colored product. The absorbance of the reaction mixture was measured spectrophotometrically at 412 nm [47].

2.5.14. Brain Microsomes Isolation

Brain microsomes were prepared using differential centrifugation. Briefly, brain tissue was homogenized in an appropriate isotonic buffer (9 volume parts Tris buffer: 0.1 mM Dithiothreitol, 0.1 mM Phenylmethylsulfonyl fluoride, 0.2 mM EDTA, 1.15% KCl and 20% (*v*/*v*) glycerol (pH 7.4), and the homogenate was subjected to sequential centrifugation steps at 17,000× *g* for 30 min to remove nuclei, mitochondria, and other cellular debris. The resulting supernatant was further centrifuged at high speed (100,000× *g* for 1 h) to pellet the microsomal fraction, which was collected and resuspended in buffer for subsequent biochemical analyses [48].

2.5.15. Evaluation of MDA in Brain Microsomes

Malondialdehyde (MDA) levels in brain microsomes were determined after the incubation period by terminating the reaction with 0.5 mL of 20% trichloroacetic acid, followed by the addition of 0.5 mL of 0.67% thiobarbituric acid. The subsequent steps were carried out to quantify MDA formation spectrophotometrically. The ongoing reactions are associated with the formation of a colored complex between the malondialdehyde formed and

thiobarbituric acid. The determination of MDA was spectrophotometric at 535 nm. A molar extinction coefficient of 1.56×10^5 M^{-1} cm^{-1} was used for the calculation [49].

2.6. Preparation of Polymeric Micelles by Nanoprecipitation

PROTOCOL A. A copolymer solution (5 mg of copolymer in 5 mL of methanol) was added dropwise to purified water (5 mL) at room temperature under vigorous stirring (1000 rpm). After 30 min, the organic solvent was evaporated under reduced pressure at 37 °C to obtain a slightly opalescent, colorless micellar dispersion with a concentration of 1 mg/mL.

PROTOCOL B. Identical to Protocol A, except that the copolymer (5 mg) was dissolved in 2 mL methanol prior to dropwise addition to 5 mL water. The final micellar dispersion had the same copolymer concentration (1 mg/mL).

3. Results and Discussion

3.1. Synthesis and Characterization of Amphiphilic Copolymers Comprising Comb-like and Coil-Comb Chain Architectures

To design amphiphilic copolymers with *comb-like* and *coil-comb* chain architectures, we synthesized a series of conjugates consisting of a main chain based on random or block copolymers of styrene and 4-chloromethylstyrene, and side chains of polyglycidol. The conjugates were prepared by grafting via copper-catalyzed azide-alkyne *click* reaction of monoalkyne-functionalized PEEGE (protected polyglycidol) to azide derivatized random and block copolymers of styrene and 4-chloromethylstyrene, followed by deprotection of the ethoxyethyl protecting groups of the glycidol units with $AlCl_3.6H_2O$ (Scheme 1 and Scheme S3 in Supplementary Materials). In the first step, random P(S-*ran*-CMS) and block PS-*block*-PCMS copolymers were prepared by nitroxide-mediated controlled radical polymerization as described elsewhere [37,39] (Table S1, Scheme S1, Figures S1 and S2 in Supplementary Materials). Azide functional groups were introduced by treating the copolymers with sodium azide, thus obtaining PN_3MS-*block*-PS and P(S-*ran*-N_3MS), (Scheme S1, Figures S1 and S2 in Supplementary Materials).

Monofunctional PEEGE bearing a hydroxyl end group was prepared by ring-opening anionic polymerization of EEGE (Scheme S2, Figures S3–S6 in the Supplementary Materials), as described elsewhere [28]. At the end of EEGE polymerization, a given amount of propylene oxide was added to the reaction mixture. By this manner, a very short poly(propylene oxide) spacer (n = 4) was introduced, as confirmed by ^{1}H NMR analysis (see Section II and Figure S4 in the Supplementary Materials), allowing in the next step complete esterification with 4-pentynoic acid of PEEGE. ^{1}H NMR and SEC analyses confirmed the successful modification and formation of well-defined monoalkyne functional PEEGE macroreagent with a narrow molar mass distribution (Figures S3 and S4 in the Supplementary Materials).

In the final step, the as prepared monoalkyne-terminated PEEGE was grafted to poly(4-azidomethylstyrene) moieties of PS-*block*-PN_3MS and P(S-*ran*-N_3MS) by copper-catalyzed azide-alkyne cycloaddition (CuAAC), as presented in Scheme 1a and Scheme S3a. We aimed for a grafting density corresponding to 5–8 PEEGE chains per copolymer chain (approximately 1 graft per 2000 g/mol of backbone), as this provides sufficient hydrophilicity for micelle stabilization while preventing aggregation and steric overcrowding. Since the azido groups in the poly(azidomethylstyrene) backbones of P(S-*ran*-N_3MS) and PS-*block*-PN_3MS were in large excess relative to the alkyne groups of the PEEGE precursor (Scheme 1a), the reaction proceeded quantitatively, with complete consumption of the PEEGE derivative. Therefore, additional purification steps were not necessary. Indeed, the SEC chromatograms of the obtained copolymers are monomodal and clearly shifted to a

lower retention time (indicating the increased molar mass) as compared to the traces of the precursors (Table 1 and Table S1, Figure 1 and Figure S7).

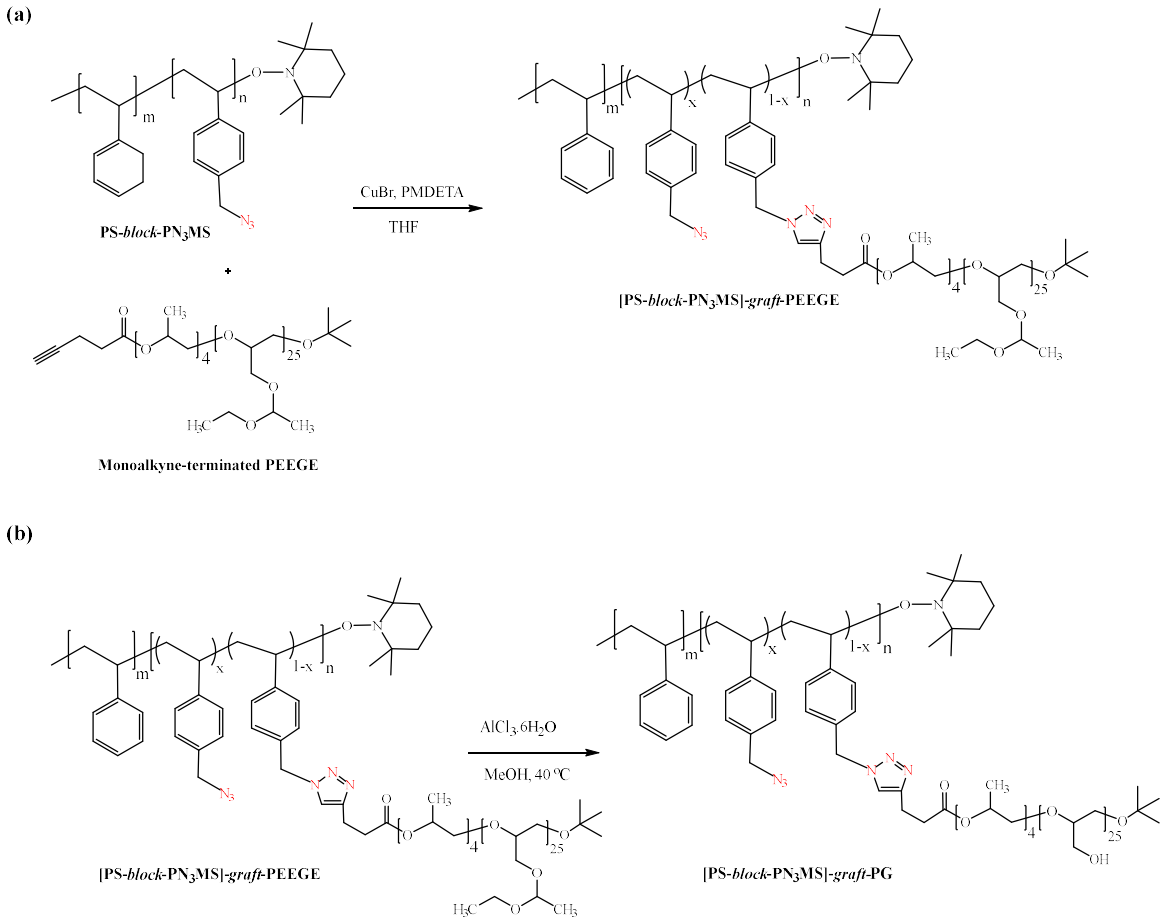

Scheme 1. Schematic representation of the (**a**) synthesis of [PS-*block*-PN_3MS]-*graft*-PEEGE copolymer by copper-catalyzed click coupling reaction and (**b**) subsequent deprotection leading to the amphiphilic [PS-*block*-PN_3MS]-*graft*-PG copolymer.

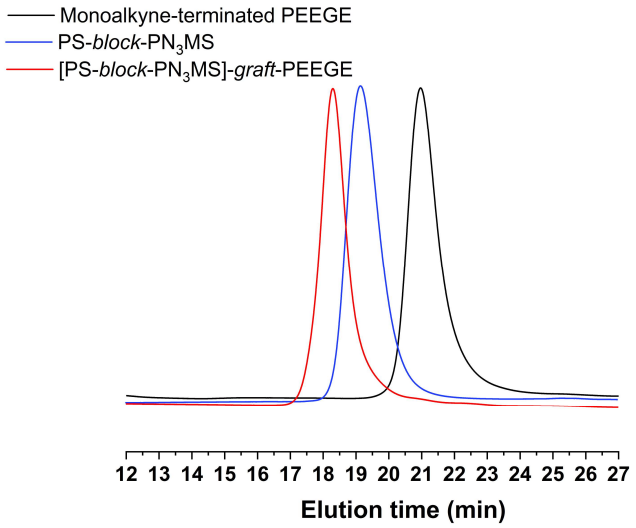

Figure 1. SEC curves of monoalkyne-terminated PEEGE, PS-*block*-PN_3MS and resulting [PS-*block*-PN_3MS]-*graft*-PEEGE copolymer.

Table 1. Characterization data of the prepared copolymers comprising comb-like and coil-comb chain architecture using azide-alkyne click chemistry approach.

Sample Code	M_{nSEC} (g/mol)	M_{wSEC} (g/mol)	$Đ$	M_{nNMR} (g/mol)
[P(S-*ran*-N_3MS)]-*graft*-PEEGE	41,220	45,540	1.10	35,610
[P(S-*ran*-N_3MS)]-*graft*-PG	-	-	-	21,480
[PS-*block*-PN_3MS]-*graft*-PEEGE	27,670	38,800	1.40	40,250
[PS-*block*-PN_3MS]-*graft*-PG	-	-	-	24,220

In addition, the ^{1}H NMR spectra of the obtained copolymers showed all characteristic peaks for polystyrene around 1.2–1.8 ppm and 6.4–7.1 ppm, as well as for PEEGE grafted chains at 1.0–1.5 ppm, 3.2–3.7 ppm and 4.5 ppm (Figure 2 and Figure S8 in Supplementary Materials).

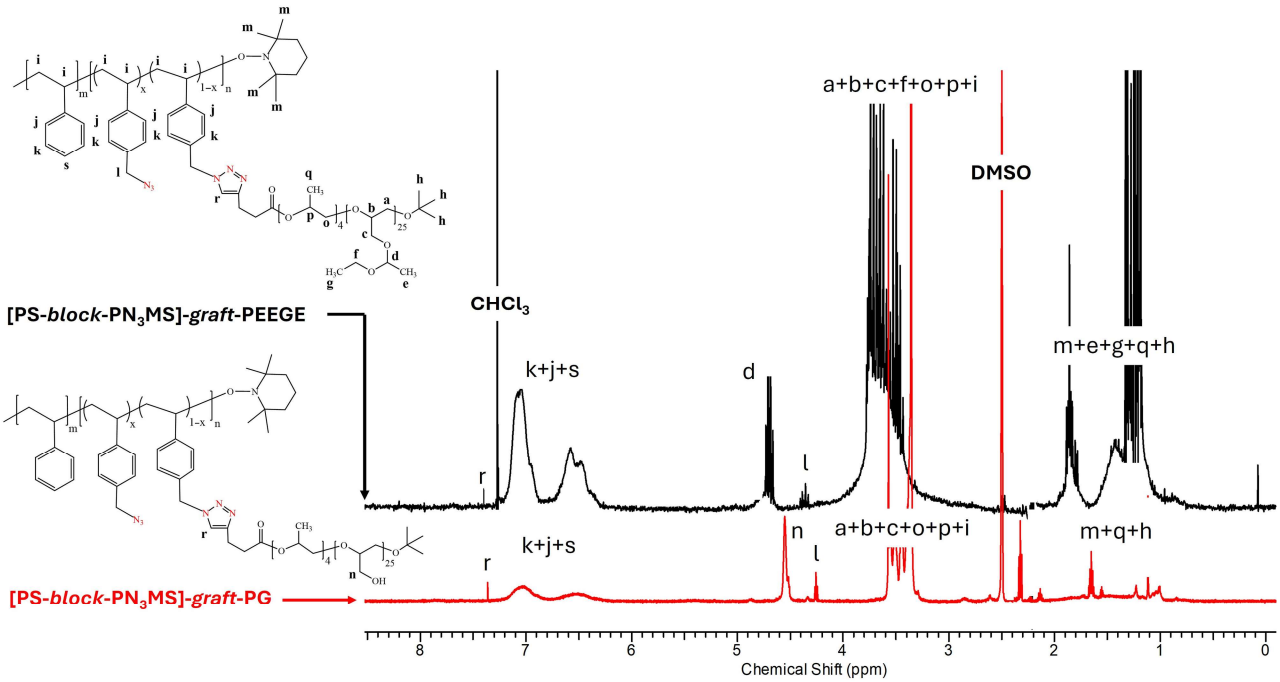

Figure 2. ^{1}H NMR spectra of the [PS-*block*-PN_3MS]-*graft*-PEEGE in $CDCl_3$ and [PS-*block*-PN_3MS]-*graft*-PG in DMSO-d_6 (600 MHz).

The grafting densities were further evaluated by integration of the triazole proton signals (7.5–7.3 ppm) relative to the aromatic protons of the polystyrene backbone in the ^{1}H NMR spectra. The experimental values $N_{graft,exp}$ were in good agreement with the theoretical numbers obtained from the feed ratios $N_{graft,theor}$, i.e., ≈5 grafts per chain for the random copolymer and ≈8 grafts per chain for the block copolymer (see Section V in the Supplementary Materials). This agreement confirms the high efficiency of the CuAAC coupling and validates the designed grafting densities.

Finally, the protective ethoxyethyl groups of PEEGE were cleaved (Scheme 1b and Scheme S3b in the Supplementary Materials), leading to well-defined amphiphilic [P(S-*ran*-N_3MS)]-*graft*-PG and [PS-*block*-PN_3MS]-*graft*-PG copolymers comprising comb-like and coil-comb chain architecture (Table 1, Figure 2 and Figure S8 in the Supplementary Materials). The conversion of the PEEGE chains into PG ones at the selected conditions was confirmed by ^{1}H NMR analysis, where complete disappearance of the signals assigned to the methyl at 1.2 ppm and methine protons at 4.7 ppm from the protective ethoxyethyl

group was observed (Figure 2 and Figure S8 in the Supplementary Materials). In addition, a new signal assigned to OH groups of PG was detected at 4.5 ppm.

3.2. Aqueous Solution Properties

The synthesized copolymers are not directly soluble in water; therefore, the solvent evaporation method was employed to obtain well-defined nanoparticles. The [P(S-*ran*-N_3MS)]-*graft*-PG and [PS-*block*-PN_3MS]-*graft*-PG were dissolved in methanol. The resulting solutions were then added dropwise to ultrapure water under vigorous stirring at room temperature. Finally, the organic solvent was removed under vacuum, yielding slightly opalescent, colorless solutions with a copolymer stock concentration of 1 mg/mL. One way to characterize the formation of micelles is by determining the critical micelle concentrations (CMCs) using a standard procedure, with the hydrophobic dye 1,6-diphenyl-1,3,5-hexatriene (DPH) as a probe [6,8,13]. For this purpose, the stock dispersions were diluted into a series of aqueous solutions covering the concentration range 9.76×10^{-4}–1.0 mg/mL. DPH shows very weak absorbance in water. However, when incorporated into the hydrophobic micellar core, it exhibits a characteristic absorption band at 356 nm. The increase in the intensity of this band with polymer concentration is used to determine the CMC (Figure 3).

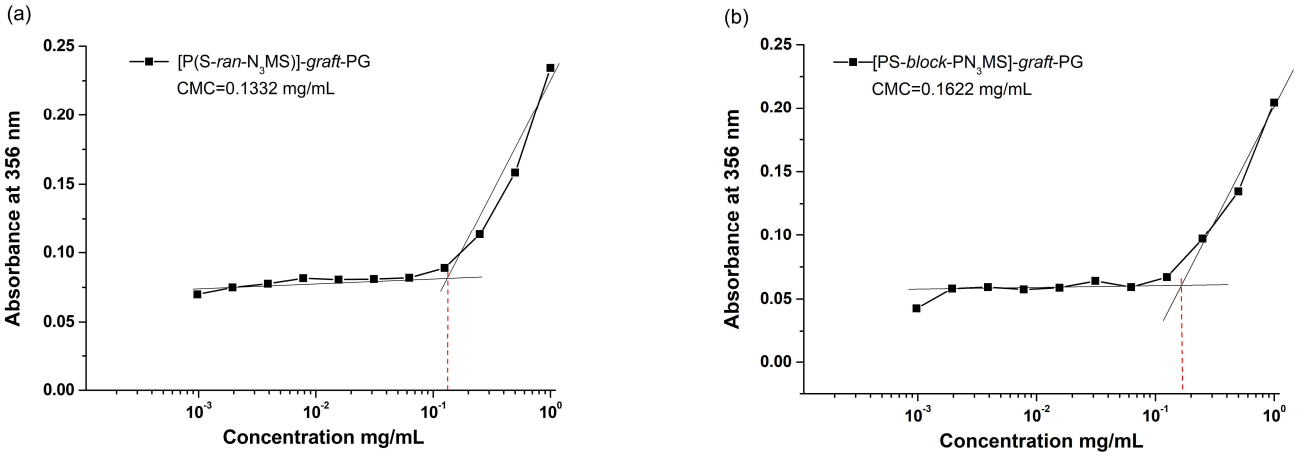

Figure 3. Determination of CMC of the amphiphilic copolymers comprising comb-like and coil-comb chain architecture: (**a**) [P(S-*ran*-N_3MS)]-*graft*-PG and (**b**) [PS-*block*-PN_3MS]-*graft*-PG using DPH absorbance at 356 nm in aqueous media at 37 °C.

Given the expected kinetic stability of micelles with polystyrene cores, the prepared samples were analyzed by UV–vis spectrophotometry after 24 h of incubation in the dark and again after 72 h. The CMC values of 0.13 mg/mL for [P(S-*ran*-N_3MS)]-*graft*-PG and 0.16 mg/mL for [PS-*block*-PN_3MS]-*graft*-PG were identified as the break in the absorbance versus copolymer concentration curves, as shown in Figure 3 and Figure S9. Each value represents the average of three independent measurements. These values are comparable to those reported for amphiphilic block copolymers with similar hydrophilic/hydrophobic balance, confirming the effective self-assembly of the synthesized systems [2,13,15]. Consistent with the glassy nature of the polystyrene core, micellar dissociation in these systems is kinetically hindered, allowing assemblies to persist upon dilution below the CMC on experimentally relevant timescales.

Further, the micellar assembly of comb-like [P(S-*ran*-N_3MS)]-*graft*-PG and coil-comb [PS-*block*-PN_3MS]-*graft*-PG copolymers was investigated by dynamic and electrophoretic light scattering (Figure 4, Table 2 and Scheme 2).

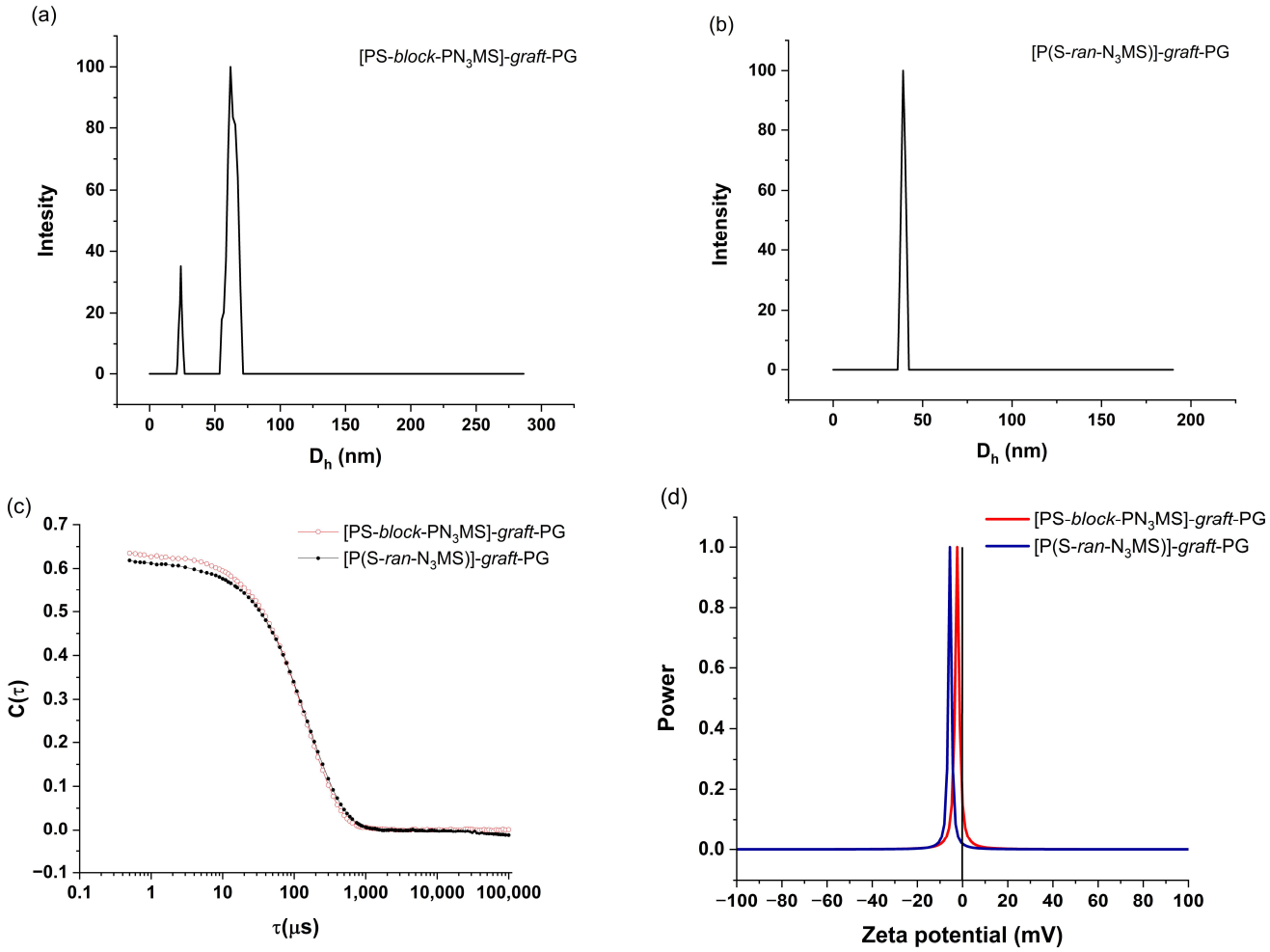

Figure 4. Hydrodynamic diameter (D_h) distributions of polymeric micelles prepared by nanoprecipitation: (**a**) [PS-*block*-PN$_3$MS]-*graft*-PG and (**b**) [P(S-*ran*-N$_3$MS)]-*graft*-PG. (**c**) Representative intensity correlation functions C(τ) from DLS measurements. (**d**) ζ-potential profiles (red line—[PS-*block*-PN$_3$MS]-*graft*-PG; blue line—[P(S-*ran*-N$_3$MS)]-*graft*-PG).

Table 2. Dynamic and electrophoretic light scattering characterization data of the micelles prepared from [P(S-*ran*-N$_3$MS)]-*graft*-PG and [PS-*block*-PN$_3$MS]-*graft*-PG copolymers. Measurements were performed in water at 37 °C and a scattering angle of 90° at a polymer concentration of 1 mg/mL. Values are presented as mean ± SD (n = 3).

Copolymer	D_h (nm)				ζ-Potential (mV)			
					PALS		ELS	
	Prot. A	PDI	Prot. B	PDI	Prot. A	Prot. B	Prot. A	Prot. B
P[(S-*ran*-N$_3$MS)]-*graft*-PG	39 ± 3	0.13	47 ± 4	0.16	−6.8 ± 0.5	−6.2 ± 0.5	−4.9 ± 0.9	−5.7 ± 1.4
[PS-*block*-PN$_3$MS]-*graft*-PG	23 ± 3 and 61 ± 2	0.2	32.0 ± 2 and 92 ± 5	0.25	−5.2 ± 0.3	−3.8 ± 1.5	−1.5 ± 1.1	−2.1 ± 1.2

In an effort to obtain well-defined nanoparticles with a monomodal size distribution, two different nanoprecipitation-based preparation protocols (Protocol A and Protocol B) were employed. Notably, Protocol A reproducibly yielded smaller micelles compared to Protocol B, while both methods produced micelles with comparable ζ-potentials (Table 2 and Figure 4). This observation suggests that the solvent-to-water ratio during nanoprecipitation plays a decisive role in controlling micelle size, in line with previous reports on

amphiphilic block copolymers [13]. Importantly, the persistence of bimodal size distributions irrespective of the nanoprecipitation protocol (Protocol A and Protocol B) indicates that this behavior is governed by copolymer topology rather than by preparation conditions. Representative intensity correlation functions are shown in Figure 4c, confirming the reliability of the DLS analysis.

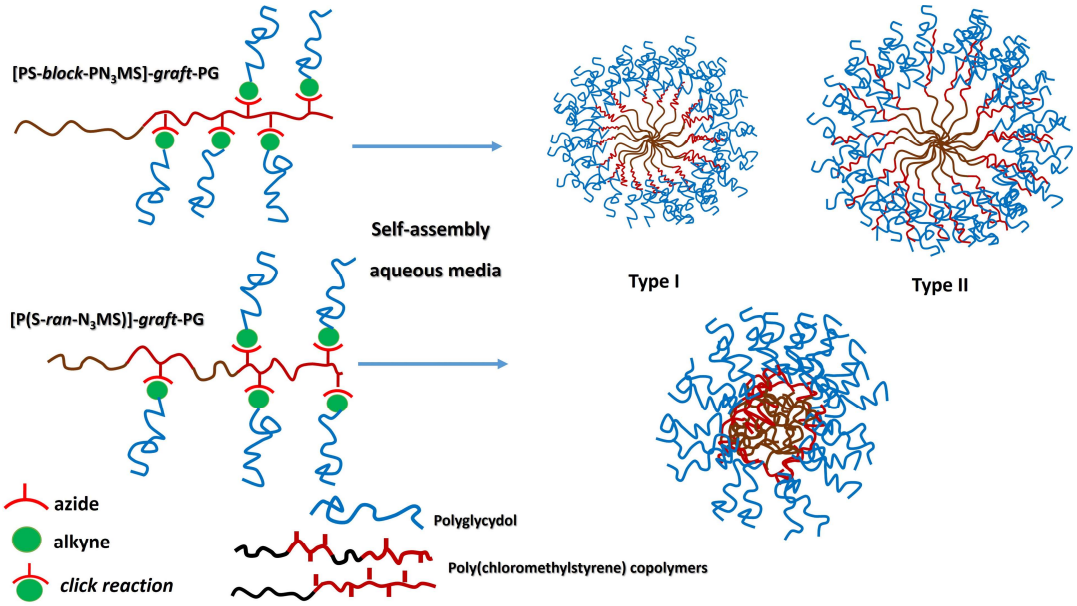

Scheme 2. Schematic representation of the polymeric micelles: models illustrating two types (I and II) of micelle assembly of the coil-comb [PS-*block*-PN$_3$MS]-*graft*-PG copolymer; model illustrating micelle assembly of the comb-like [P(S-*ran*-N$_3$MS)]-*graft*-PG copolymer.

According to Wang et al. [17], the formation of micelles in block copolymer systems is governed by the competition between block lengths and solvent selectivity, which can result in the coexistence of two distinct micelle types. In the present study, we observe a similar behavior in block PS-*block*-PN$_3$MS copolymer grafted with polyglycidol. This block copolymer exhibits a bimodal micelle size distribution, a behavior observed under both preparation protocols, indicating the presence of two thermodynamically stable micellar populations, likely corresponding to different core–corona arrangements (Figure 4a). In contrast, the random P(S-*ran*-N$_3$MS) copolymer grafted with the same polyglycidol chains forms a uniform, monomodal micelle population (Figure 4b). This difference reflects the reduced block segregation in the random copolymers, which favors the formation of a single type of micelle with homogeneous core and corona structures. Moreover, as discussed by Wang et al., the number of grafted side chains also plays an important role: while copolymers with $n \leq 8$ mainly form type I micelles, those with $n \geq 12$ can form both types I and II, whereas intermediate values ($8 < n < 12$) are predicted to yield a single mixed population (a micelle type with mixed core–corona characteristic). With ~8 grafts per chain, our block copolymer lies at this borderline; however, instead of one such mixed population, we observed two distinct micellar populations (Figure 4). This deviation suggests that the interplay of block architecture and grafting density may promote stabilization of both morphologies.

Overall, these results highlight the critical role of chain architecture and grafting in determining micellar morphology and size distribution. A schematic model was constructed to illustrate the micelle assemblies: two types (I and II) of micelles formed by the coil-comb [PS-*block*-PN$_3$MS]-*graft*-PG copolymer and the single-type micelle formed by the comb-like [P(S-*ran*-N$_3$MS)]-*graft*-PG copolymer (Scheme 2).

The PDI values further supported these observations. For the block copolymer [PS-*block*-PN$_3$MS]-*graft*-PG, PDI values were in the range of 0.20–0.25, which are usually interpreted as nearly uniform, but in this case, they reflect the coexistence of two micellar populations, consistent with the bimodal DLS curves (Figure 4). In contrast, the random copolymer [P(S-*ran*-N$_3$MS)]-graft-PG showed monomodal assemblies with narrower dispersity and PDI values $\leq$ 0.16, confirming the absence of a second particle population.

The ζ-potentials of both block PS-*block*-PN$_3$MS and random P(S-*ran*-N$_3$MS) copolymers grafted with polyglycidol are weakly negative (Figure 4d and Table 2). PALS measurements (Protocol A) yield –5 mV for the block and –6 mV for the random copolymers, while ELS (Protocol A) measurements give –1.5 mV and –4.9 mV, respectively. The overall low magnitude of the ζ-potentials indicates minimal electrostatic repulsion, suggesting that steric stabilization provided by the polyglycidol grafts dominates micelle stability. Because the PG grafts introduce multiple polar surface functionalities (mainly hydroxyl groups together with a small number of triazole units), the slightly less negative values observed for the block copolymer, particularly in ELS, likely reflect partial shielding of these groups within the denser corona of the bimodal micelles, whereas the random copolymer, with a more uniform distribution of grafts, maintains higher surface exposure of polar functionalities. These findings support the idea that chain architecture not only influences micelle size distribution but also affects surface charge characteristics and colloidal behavior.

Additionally, AFM was performed to characterize the morphology of the prepared micelles (Figure 5). The objects appeared well-separated and predominantly spherical, with dimensions in the dry state that were consistent with those obtained by dynamic light scattering.

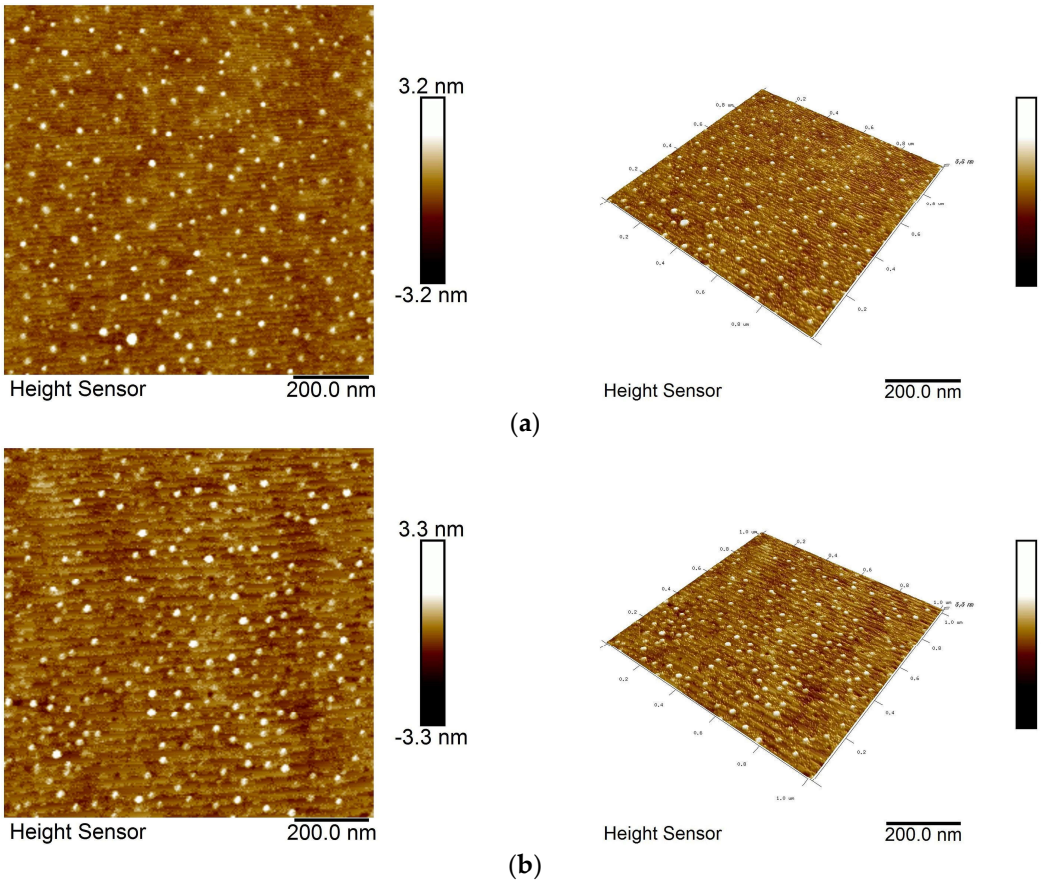

Figure 5. Representative AFM images of micelles deposited from 1 mg/mL aqueous solution: (**a**) [P(S-*ran*-N$_3$MS)]-*graft*-PG; (**b**) [PS-*block*-PN$_3$MS]-*graft*-PG.

The observed morphology confirms the formation of well-defined spherical structures, suggesting that the polyglycidol corona maintains its steric stabilization even in the dry state. While AFM provides valuable insight into the nanoscale surface topography of the deposited particles, it does not resolve the full size distribution present in solution; therefore, complementary DLS measurements are essential to distinguish between monomodal and bimodal populations. Taken together, these findings demonstrate that the combination of steric stabilization by the grafted corona and block architecture governs both the morphology and the colloidal behavior of the micelles.

3.3. In Vitro Biocompatibility Evaluation of the Copolymer-Based Nanocarriers

The lack of cytotoxicity is a mandatory requirement for all materials, including polymers, intended for use as excipients in drug-carrier formulations. In this regard, the cytotoxic potential of the newly synthesized copolymers [P(S-*ran*-N_3MS)]-*graft*-PG and [PS-*block*-PN_3MS]-*graft*-PG was evaluated in a panel of cellular models that collectively represent key biological barriers and tissue types likely to be exposed to the polymeric nanocarriers following different administration routes. Considering the expected kinetic stability of micelles with polystyrene cores, the following biological assays were conducted over a broad concentration range, including nominal concentrations below the CMC. These included normal fibroblasts (L929), myeloid leukemia cells (HL-60), endothelial cells (Ea.hy926), and neuronal cells (SH-SY5Y). In addition, neurotoxicity was further examined in isolated rat brain subcellular fractions. This multilevel approach enabled the assessment of potential adverse effects in systems relevant for systemic and intravascular exposure (HL-60 and Ea.hy926), topical or subcutaneous delivery (L929 fibroblasts), and CNS-targeted applications (SH-SY5Y cells together with synaptosomal, mitochondrial, and microsomal fractions). Cells were treated with varying concentrations of the tested copolymers (0.1–200 μg/mL) to cover levels both below and above the CMC of the copolymers. Analyzing all systems under standardized conditions ensured a comprehensive and comparable evaluation of biocompatibility.

L929 fibroblasts, which are known to be highly responsive to toxic insults from various chemical and biological agents and are therefore considered a reliable indicator of cellular sensitivity [50,51], exhibited no reduction in viability after 24 h exposure across the full concentration range tested (0.1–200 μg/mL). Both copolymers preserved fibroblast metabolic activity, confirming their safety for potential dermal or subcutaneous administration (Figure 6a). The observed slightly elevated cell viability values above 100% reflect continued cell proliferation relative to the control, which is commonly observed in metabolic activity assays for biocompatible polymeric systems.

Similarly, neither the copolymers nor the micelles formed thereof affected viability in Ea.hy926 endothelial cells (Figure 6b). This cell line is a widely accepted in vitro model of the vascular endothelium, frequently used for assessing biocompatibility, inflammatory activation, and interactions with nanomaterials or drug-delivery systems [52]. Because endothelial tissues form the first biological interface following systemic or intravascular application, these findings strongly support the safe use of the tested copolymers for intravenous administration.

To evaluate potential neurotoxicity relevant for CNS-directed delivery, the copolymers were examined in SH-SY5Y neuronal cells, a well-established human neuroblastoma-derived model [53]. Cells were exposed to the micellar systems for 24 h under the same conditions. Both formulations maintained high viability across all concentrations tested, indicating excellent neuronal compatibility and suggesting minimal risk of neurotoxicity in vitro (Figure 6c).

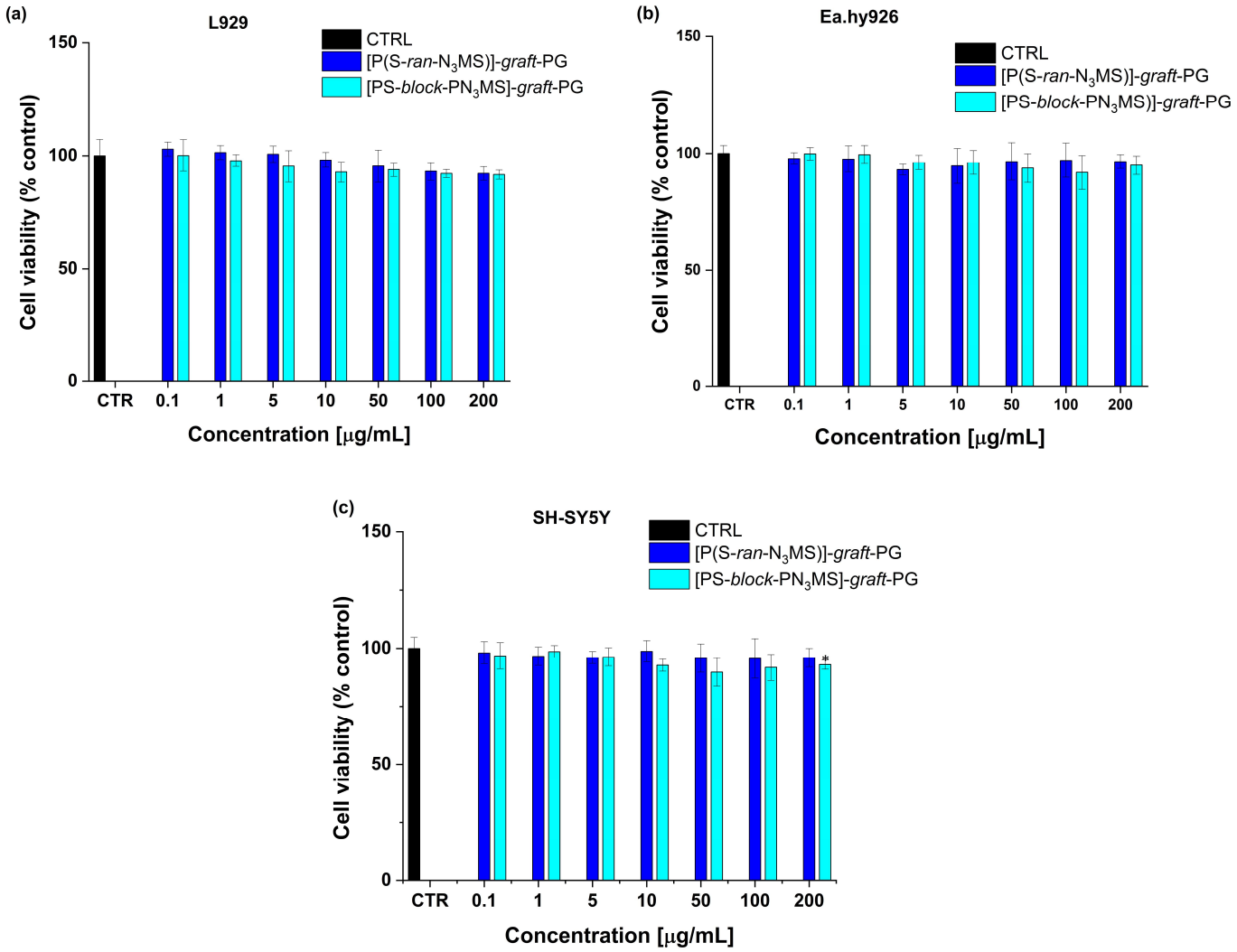

Figure 6. In vitro evaluation of the cytotoxicity of [P(S-*ran*-N_3MS)]-*graft*-PG and [PS-*block*-PN_3MS]-*graft*-PG (0.1, 1, 5, 10, 25, 50, 100, 200 μg/mL) on L929 (**a**), Ea.hy926 (**b**), and SH-SY5Y (**c**) cells 24 h post-treatment, using the MTT assay. * $p < 0.05$. Statistical analysis was performed using one-way ANOVA followed by Dunnett's post hoc test. Data are presented as percentages relative to untreated cells and expressed as mean ± SD (n = 8).

To further characterize the biocompatibility of the copolymers and to broaden the spectrum of tested cell types, additional experiments extending to 72 h were performed. For this purpose, concentration–response curves were obtained in L929 fibroblasts and HL-60 myeloid leukemia cells. While L929 serves as a standard non-transformed cellular model for evaluating general cytocompatibility, HL-60 cells represent circulating myeloid cells that would be among the first immune-competent cells to encounter the nanocarriers after systemic administration. Including HL-60 cells therefore provides insight into potential interactions with hematological components and allows assessment of unintended cytotoxicity within the bloodstream. Importantly, the incubation period with both cell lines was prolonged to 72 h. This extended exposure was incorporated to capture potential delayed or cumulative toxic effects, which may arise from slower polymer internalization, intracellular trafficking, metabolic processing, or prolonged nanoparticle–cell interactions. Short-term assays alone may overlook these more subtle, time-dependent responses; thus, the 72 h evaluation offers a more stringent and conservative assessment of long-term biocompatibility.

The resulting concentration–effect curves, expressed as percentages of untreated controls, are presented in Figure 7. Across the tested range (20–200 μg/mL), both copolymers exhibited excellent cytocompatibility, with cell viability between 80–96%. In L929 fibroblasts, slight differences in response were observed between the two polymers, likely due to their distinct architectures. Variations in macromolecular structure can influence micellar morphology, surface properties, and interactions with cell membranes, explaining the observed differences in metabolic activity [54]. According to ISO 10993-5:2009 [54], cell viability above 80% is classified as non-cytotoxic, confirming that both [P(S-*ran*-N_3MS)]-*graft*-PG and [PS-*block*-PN_3MS]-*graft*-PG are intrinsically biocompatible even under extended exposure conditions.

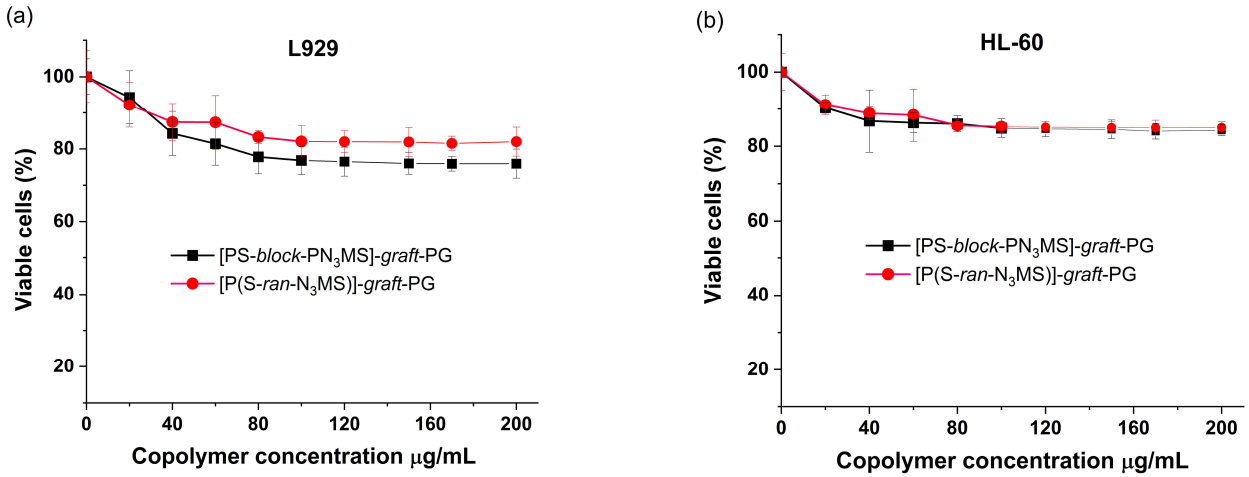

Figure 7. Concentration–response curves established by the MTT-dye reduction assay after 72 h of continuous exposure: (**a**) mouse fibroblast cells (L929) and (**b**) human acute myeloid leukemia (HL-60) cell line. Each data point represents an average arithmetic value ± standard deviation of at least 3 independent experiments.

3.4. In Vitro Neurotoxicity Evaluation in Rat Brain Sub-Cellular Fractions

To complement the cell-based assays and provide deeper mechanistic insight into potential neurotoxic effects, the micellar systems were further evaluated in isolated rat brain sub-cellular fractions, including synaptosomes, mitochondria, and microsomes. These structures are highly sensitive to metabolic disturbances, oxidative stress, and membrane damage-key indicators of early neurotoxicity.

Synaptosomes, mitochondria, and microsomes were incubated for 2 h with [PS-*block*-PN_3MS]-*graft*-PG and [P(S-*ran*-N_3MS)]-*graft*-PG across a wide concentration range (0.1–500 μg/mL), below and above CMC. Neither of the copolymers tested induced statistically significant changes in synaptosomal viability, reduced glutathione (GSH) levels, or lipid peroxidation (MDA production) (Tables 3–5). Synaptosomal viability remained near control values, mitochondrial oxidative markers were stable, and microsomal membrane integrity was preserved—indicating that neither micellar system triggers oxidative stress or metabolic impairment in neuronal sub-cellular structures.

Across all tested biological systems –normal fibroblasts, leukemia cells, endothelial and neuronal lines, and brain sub-cellular fractions—the copolymers and their micellar formulations consistently exhibited excellent biocompatibility. The convergence of evidence from multiple independent models strongly supports their safety and suitability for several major drug administration routes.

Table 3. Effects of [PS-*block*-PN_3MS]-*graft*-PG and [P(S-*ran*-N_3MS)]-*graft*-PG, at concentrations 0.1 μg/mL–500 μg/mL, on synaptosomal viability and level of reduced glutathione (GSH) in brain synaptosomes.

Group	Concentration (μg/mL)	Synaptosomal Viability, %	Level of GSH, nmol/0.1 mg Protein
Control	0	100 ± 6.5	20 ± 2.5
[PS-*block*-PN_3MS]-*graft*-PG	0.1	100 ± 3.3	20 ± 1.9
	1	100 ± 2.2	20 ± 1.8
	10	100 ± 2.9	20 ± 2.1
	100	99 ± 3.1	19 ± 2.3
	250	98 ± 3.8	18 ± 4.1
	500	96 ± 4.1	18 ± 3.3
[P(S-*ran*-N_3MS)]-*graft*-PG	0.1	100 ± 2.2	20 ± 3.2
	1	100 ± 3.1	20 ± 3.6
	10	100 ± 4.4	20 ± 4.2
	100	98 ± 4.8	19 ± 4.4
	250	96 ± 5.1	18 ± 2.9
	500	95 ± 5.5	18 ± 2.7

Table 4. Effects of [PS-*block*-PN_3MS]-*graft*-PG and [P(S-*ran*-N_3MS)]-*graft*-PG, at concentrations 0.1 μg/mL–500 μg/mL, on level of reduced glutathione (GSH) and production of malondialdehyde (MDA) in brain mitochondria.

Group	Concentration (μg/mL)	MDA Production, nmol/0.1 mg Protein	Level of GSH, nmol/0.1 mg Protein
Control	0	0.111 ± 0.01	20 ± 2.5
PS-*block*-PN_3MS]-*graft*-PG	0.1	0.119 ± 0.01	19 ± 2.2
	1	0.119 ± 0.01	19 ± 1.9
	10	0.119 ± 0.01	19 ± 2.5
	100	0.121 ± 0.01	18 ± 2.7
	250	0.125 ± 0.01	18 ± 3.9
	500	0.131 ± 0.01	17 ± 3.8
[P(S-*ran*-N_3MS)]-*graft*-PG	0.1	0.118 ± 0.01	20 ± 1.8
	1	0.118 ± 0.01	20 ± 1.9
	10	0.118 ± 0.01	20 ± 2.1
	100	0.117 ± 0.01	19 ± 3.3
	250	0.117 ± 0.01	19 ± 3.8
	500	0.117 ± 0.01	19 ± 4.4

Table 5. Effects of [PS-*block*-PN_3MS]-*graft*-PG and [P(S-*ran*-N_3MS)]-*graft*-PG, at concentrations 0.1 μg/mL–500 μg/mL: 0.1 μg/mL, 1 μg/mL, 10 μg/mL, 100 μg/mL, 250 μg/mL and 500 μg/mL, on production of malondialdehyde (MDA) in brain microsomes.

Group	Concentration (μg/mL)	MDA Production, nmol/0.1 mg Protein
Control		0.113 ± 0.01
[PS-*block*-PN_3MS]-*graft*-PG	0.1	0.114 ± 0.01
	1	0.114 ± 0.01
	10	0.114 ± 0.01
	100	0.122 ± 0.01
	250	0.128 ± 0.01
	500	0.129 ± 0.01

Table 5. *Cont.*

Group	Concentration (μg/mL)	MDA Production, nmol/0.1 mg Protein
[P(S-*ran*-N_3MS)]-*graft*-PG	0.1	0.115 ± 0.01
	1	0.115 ± 0.01
	10	0.115 ± 0.01
	100	0.118 ± 0.01
	250	0.119 ± 0.01
	500	0.119 ± 0.01

4. Conclusions

In this study, two amphiphilic copolymers with distinct macromolecular topologies, namely [P(S-*ran*-N_3MS)]-*graft*-PG and [PS-*block*-PN_3MS]-*graft*-PG, were successfully synthesized and comprehensively characterized. Both systems exhibited low critical micelle concentrations (0.13 and 0.16 mg/mL) and formed self-assembled nanoparticles with average sizes of 39 nm and 92 nm, respectively, narrow size distributions (PDI < 0.2), and nearly neutral zeta potentials. At the investigated grafting density, the different chain architectures led to distinct micellar organization, with the block copolymer exhibiting bimodal micellar populations, whereas the random copolymer formed uniform, monomodal assemblies. Taken together, the physicochemical characteristics and kinetically stabilized nature of the PS-based micelles support their prospective use as drug delivery carriers, owing to enhanced colloidal stability and reduced nonspecific interactions upon dilution. The newly synthesized copolymers and their corresponding micellar formulations demonstrated excellent biocompatibility, showing no detectable cytotoxicity over a wide concentration range in representative human cell lines, including fibroblasts, endothelial, neuronal, and leukemia cells, even after prolonged exposure. In vitro investigations using isolated rat brain subcellular fractions further confirmed the absence of neurotoxic effects.

Collectively, these findings support the safety of the investigated copolymers and highlight their potential as versatile platforms for systemic, topical, and CNS-targeted drug delivery. On this basis, the present study indicates that [P(S-*ran*-N_3MS)]-*graft*-PG and [PS-*block*-PN_3MS]-*graft*-PG represent promising materials for the development of drug delivery carriers devoid of inherent cytotoxic potential.

Supplementary Materials: The following Supplementary Materials can be downloaded at https://www.mdpi.com/article/10.3390/polym18040517/s1, Scheme S1. Synthesis and azide modification of P(S-*ran*-CMS) (a) and PS-*block*-PCMS (b); Table S1. Characterization data of the random P(S-*ran*-CMS) and block PS-*block*-PCMS copolymers; Figure S1. SEC curves of (a) the initial P(S-*ran*-CMS) and azide-functionalized intermediate P(S-*ran*-N_3MS), and (b) the initial PS-*block*-PCMS and the corresponding azide- functionalized intermediate PS-*block*-PN_3MS (RI trace, THF); Figure S2. ^{1}H NMR spectra (600 MHz in $CDCl_3$) of (a) the initial P(S-*ran*-CMS) and azide-functionalized P(S-*ran*-N_3MS) and (b) the initial PS-*block*-PCMS copolymer and the corresponding azide-functionalized PS-*block*-PN_3MS; Scheme S2. Schematic presentations of the synthesis of monoalkyne-terminated PEEGE via esterification of monohydroxyl-terminated PEEGE with 4-pentynoic acid.; Figure S3. SEC chromatograms of monohydroxyl-terminated PEEGE (1, red trace) and monoalkyne-terminated PEEGE (2, black trace) recorded in THF (RI detector); Figure S4: ^{1}H NMR spectra (600 MHz) of monohydroxyl-terminated PEEGE (red) in $CDCl_3$ and monoalkyne-terminated PEEGE (black) in CD_3OD; Figure S5. FTIR spectra of monohydroxyl-terminated PEEGE (1) and monoalkyne-terminated PEEGE (2); Figure S6. ^{1}H NMR spectra (600 MHz) of monohydroxyl-terminated PEEGE (black) in $CDCl_3$ and the corresponding deprotected polyglycidol (PG) (red) in CD_3OD; Scheme S3: Schematic representation of (a) the synthesis of [P(S-*ran*-N_3MS)]-*graft*-PEEGE copolymer by copper-catalyzed click coupling reaction and (b) subsequent deprotection leading to the amphiphilic

[P(S-*ran*-N_3MS)]-*graft*-PG copolymer; Figure S7. SEC curves of monoalkyne-terminated PEEGE, P(S-*ran*-N_3MS) and resulting [P(S-*ran*-N_3MS)]-*graft*-PEEGE copolymer; Figure S8. ^{1}H NMR spectra of the [P(S-*ran*-N_3MS)]-*graft*-PEEGE in $CDCl_3$ and [P(S-*ran*-N_3MS)]-*graft*-PG in DMSO-d_6 (600 MHz); Figure S9. Determination of CMC of the amphiphilic copolymers comprising comb-like and coil-comb chain architecture: (a) [P(S-*ran*-N_3MS)]-*graft*-PG after 6 days and (b) [PS-*block*-PN_3MS]-*graft*-PG after 72 h using the DPH absorbance at 356 nm in aqueous media at 37 °C; Table S2. Molar feed ratios of monoalkyne-terminated PEEGE to azide-functional polymer chains.

Author Contributions: Conceptualization, S.R. and S.P.; methodology, N.T.-M., S.R., N.D. and D.M.; validation, N.T.-M., D.M. and S.R.; formal analysis, N.T.-M., D.M., S.R., M.K.-B., D.S. and V.T.; investigation, N.T.-M., E.D., N.D., D.M., M.K.-B., D.S. and V.T.; resources, S.R. and S.P.; data curation, N.T.-M. and N.D.; writing—original draft preparation, N.T.-M. and D.M.; writing—review and editing, N.T.-M., S.R., S.P., D.M. and E.D.; visualization, N.T.-M., D.M., D.S., M.K.-B. and V.T.; supervision, S.R.; project administration, S.R. and N.T.-M.; funding acquisition, S.R. All authors have read and agreed to the published version of the manuscript.

Funding: The support of the Centre of Competence "Sustainable Utilization of Bio-Resources and Waste of Medicinal and Aromatic Plants for Innovative Bioactive Products" (BIORESOURCES BG), project BG16RFPR002-1.014-0001, funded by the Program "Research, Innovation and Digitization for Smart Transformation" 2021–2027, co-funded by the European Union, is greatly acknowledged.

Institutional Review Board Statement: The animal study protocol was approved by the Bulgarian Food Safety Agency (Permission No. 304, valid until 28 June 2026).

Data Availability Statement: All data generated or analyzed during this study are included in this published article and its Supplementary Materials.

Acknowledgments: D.M., M.K.-B., D.S. and V.T. gratefully acknowledge the financial support provided by the European Union–NextGenerationEU through the National Recovery and Resilience Plan of the Republic of Bulgaria, project No.BG-RRP-2.004-0004-C01. Krasimira Rusinova-Ilieva is gratefully acknowledged for AFM imaging.

Conflicts of Interest: The authors declare no conflicts of interest.

Abbreviations

The following abbreviations are used in this manuscript:

PS	Polystyrene
PG	Polyglycidol
PEEGE	Poly(ethoxyethyl glycidyl ether)
PPO	Poly(propylene oxide)
CMS	Chloromethylstyrene
N_3MS	Azidomethylstyrene
CuAAC	Copper-catalyzed azide–alkyne cycloaddition
M_n	Number-average molecular weight
M_w	Weight-average molecular weight
Đ	Dispersity
SEC	Size exclusion chromatography
NMR	Nuclear magnetic resonance
CMC	Critical micelle concentration
DLS	Dynamic light scattering

References

1. Tibbitt, M.W.; Dahlman, J.E.; Langer, R. Emerging Frontiers in Drug Delivery. *J. Am. Chem. Soc.* **2016**, *138*, 704–717. [CrossRef]
2. Jiang, Z.; Liu, H.; He, H.; Ribbe, A.E.; Thayumanavan, S. Blended Assemblies of Amphiphilic Random and Block Copolymers for Tunable Encapsulation and Release of Hydrophobic Guest Molecules. *Macromolecules* **2020**, *53*, 2713–2723. [CrossRef]
3. Dutertre, F.; Gaillard, C.; Chassenieux, C.; Nicolai, T. Branched Wormlike Micelles Formed by Self-Assembled Comblike Amphiphilic Copolyelectrolytes. *Macromolecules* **2015**, *48*, 7604–7612. [CrossRef]
4. Jain, K.K. An Overview of Drug Delivery Systems. In *Drug Delivery Systems*; Jain, K.K., Ed.; Methods in Molecular Biology; Springer: New York, NY, USA, 2020; Volume 2059, pp. 1–54, ISBN 978-1-4939-9797-8.
5. Kakkar, A.; Traverso, G.; Farokhzad, O.C.; Weissleder, R.; Langer, R. Evolution of Macromolecular Complexity in Drug Delivery Systems. *Nat. Rev. Chem.* **2017**, *1*, 63. [CrossRef]
6. Perumal, S.; Atchudan, R.; Lee, W. A Review of Polymeric Micelles and Their Applications. *Polymers* **2022**, *14*, 2510. [CrossRef]
7. Toncheva-Moncheva, N.; Dimitrov, E.; Grancharov, G.; Momekova, D.; Petrov, P.; Rangelov, S. Cinnamyl-Modified Polyglycidol/Poly(ε-Caprolactone) Block Copolymer Nanocarriers for Enhanced Encapsulation and Prolonged Release of Cannabidiol. *Pharmaceutics* **2023**, *15*, 2128. [CrossRef]
8. Siebert, M.; Henke, A.; Eckert, T.; Richtering, W.; Keul, H.; Möller, M. Polystyrene-*Block*-Polyglycidol Micelles Cross-Linked with Titanium Tetraisopropoxide. Laser Light and Small-Angle X-Ray Scattering Studies on Their Formation in Solution. *Langmuir* **2010**, *26*, 16791–16800. [CrossRef]
9. Lee, S.; Saito, K.; Lee, H.-R.; Lee, M.J.; Shibasaki, Y.; Oishi, Y.; Kim, B.-S. Hyperbranched Double Hydrophilic Block Copolymer Micelles of Poly(Ethylene Oxide) and Polyglycerol for pH-Responsive Drug Delivery. *Biomacromolecules* **2012**, *13*, 1190–1196. [CrossRef]
10. Toncheva, N.; Tsvetanov, C.; Rangelov, S.; Trzebicka, B.; Dworak, A. Hydroxyl End-Functionalized Poly(2-Isopropyl Oxazoline)s Used as Nano-Sized Colloidal Templates for Preparation of Hollow Polymeric Nanocapsules. *Polymer* **2013**, *54*, 5166–5173. [CrossRef]
11. Bongiovì, F.; Fiorica, C.; Palumbo, F.S.; Di Prima, G.; Giammona, G.; Pitarresi, G. Imatinib-Loaded Micelles of Hyaluronic Acid Derivatives for Potential Treatment of Neovascular Ocular Diseases. *Mol. Pharm.* **2018**, *15*, 5031–5045. [CrossRef]
12. Bielas, R.; Maksym, P.; Tarnacka, M.; Minecka, A.; Jurkiewicz, K.; Talik, A.; Geppert-Rybczyńska, M.; Grelska, J.; Mielańczyk, Ł.; Bernat, R.; et al. Synthetic Strategy Matters: The Study of a Different Kind of PVP as Micellar Vehicles of Metronidazole. *J. Mol. Liq.* **2021**, *332*, 115789. [CrossRef]
13. Otulakowski, L.; Dworak, A.; Forys, A.; Gadzinowski, M.; Slomkowski, S.; Basinska, T.; Trzebicka, B. Micellization of Polystyrene-b-Polyglycidol in Dioxane and Water/Dioxane Solutions. *Polymers* **2020**, *12*, 200. [CrossRef]
14. Wang, W.-L.; Jin, R.-H. Synthesis and Self-Assembly of Amphiphilic Comb-Copolymers Possessing Polyethyleneimine and Its Derivatives: Site-Selective Formation of Loop-Cluster Covered Vesicles and Flower Micelles. *Polymer* **2021**, *212*, 123289. [CrossRef]
15. Ozdemir, F.; Keul, H.; Mourran, A.; Moeller, M. Polyglycidol Based Amphiphilic Double-Comb Copolymers and Their Self-Association in Aqueous Solution. *Macromol. Rapid Commun.* **2011**, *32*, 1007–1013. [CrossRef]
16. Wang, J.; Guo, K.; An, L.; Müller, M.; Wang, Z.-G. Micelles of Coil−Comb Block Copolymers in Selective Solvents: Competition of Length Scales. *Macromolecules* **2010**, *43*, 2037–2041. [CrossRef]
17. Dimitrov, E.; Toncheva-Moncheva, N.; Doumanov, J.A.; Mladenova, K.; Petrova, S.; Pispas, S.; Rangelov, S. Three-Dimensional Nucleic Acid Nanostructures Based on Self-Assembled Polymer-Oligonucleotide Conjugates of Comblike and Coil-Comb Chain Architectures. *Biomacromolecules* **2023**, *24*, 2213–2224. [CrossRef]
18. Shin, S.; Moon, S.; Seo, M.; Kim, S.Y. Synthesis of Coil-comb Block Copolymers Containing Polystyrene Coil and Poly(Methyl Methacrylate) Side Chains via Atom Transfer Radical Polymerization. *J. Polym. Sci. Part A Polym. Chem.* **2016**, *54*, 2971–2983. [CrossRef]
19. Ruokolainen, J.; Saariaho, M.; Ikkala, O.; Ten Brinke, G.; Thomas, E.L.; Torkkeli, M.; Serimaa, R. Supramolecular Routes to Hierarchical Structures: Comb-Coil Diblock Copolymers Organized with Two Length Scales. *Macromolecules* **1999**, *32*, 1152–1158. [CrossRef]
20. Webber, S.E. Polymer Micelles: An Example of Self-Assembling Polymers. *J. Phys. Chem. B* **1998**, *102*, 2618–2626. [CrossRef]
21. Nagarajan, R. "Non-Equilibrium" Block Copolymer Micelles with Glassy Cores: A Predictive Approach Based on Theory of Equilibrium Micelles. *J. Colloid Interface Sci.* **2015**, *449*, 416–427. [CrossRef]
22. Nakayama, Y.; Miyamura, M.; Hirano, Y.; Goto, K.; Matsuda, T. Preparation of Poly(Ethylene Glycol)–Polystyrene Block Copolymers Using Photochemistry of Dithiocarbamate as a Reduced Cell-Adhesive Coating Material. *Biomaterials* **1999**, *20*, 963–970. [CrossRef]
23. Yu, K.; Eisenberg, A. Multiple Morphologies in Aqueous Solutions of Aggregates of Polystyrene-*Block*-Poly(Ethylene Oxide) Diblock Copolymers. *Macromolecules* **1996**, *29*, 6359–6361. [CrossRef]
24. Angot, S.; Taton, D.; Gnanou, Y. Amphiphilic Stars and Dendrimer-Like Architectures Based on Poly(Ethylene Oxide) and Polystyrene. *Macromolecules* **2000**, *33*, 5418–5426. [CrossRef]

25. Knop, K.; Hoogenboom, R.; Fischer, D.; Schubert, U.S. Poly(Ethylene Glycol) in Drug Delivery: Pros and Cons as Well as Potential Alternatives. *Angew. Chem. Int. Ed.* **2010**, *49*, 6288–6308. [CrossRef]
26. Yang, Q.; Lai, S.K. Anti-PEG Immunity: Emergence, Characteristics, and Unaddressed Questions. *WIREs Nanomed. Nanobiotechnol.* **2015**, *7*, 655–677. [CrossRef]
27. Sellaturay, P.; Nasser, S.; Ewan, P. Polyethylene Glycol–Induced Systemic Allergic Reactions (Anaphylaxis). *J. Allergy Clin. Immunol. Pract.* **2021**, *9*, 670–675. [CrossRef]
28. Toncheva-Moncheva, N.; Bakardzhiev, P.; Rangelov, S.; Trzebicka, B.; Forys, A.; Petrov, P.D. Linear Amphiphilic Polyglycidol/Poly(ε-Caprolactone) Block Copolymers Prepared via "Click" Chemistry-Based Concept. *Macromolecules* **2019**, *52*, 3435–3447. [CrossRef]
29. Son, S.; Shin, E.; Kim, B.-S. Light-Responsive Micelles of Spiropyran Initiated Hyperbranched Polyglycerol for Smart Drug Delivery. *Biomacromolecules* **2014**, *15*, 628–634. [CrossRef]
30. Gervais, M.; Brocas, A.-L.; Cendejas, G.; Deffieux, A.; Carlotti, S. Synthesis of Linear High Molar Mass Glycidol-Based Polymers by Monomer-Activated Anionic Polymerization. *Macromolecules* **2010**, *43*, 1778–1784. [CrossRef]
31. Utrata, A.; Walach, W.; Dworak, A.; Trzebicka, B. Hydrophobically Modified Polyglycidol—The Control of Lower Critical Solution Temperature. *Polym. Bull.* **2003**, *50*, 47–54. [CrossRef]
32. Siebert, M.; Keul, H.; Möller, M. Synthesis of Well-Defined Polystyrene-Block-Polyglycidol (PS-b-PG) Block Co-Polymers by Anionic Polymerization. *Des. Monomers Polym.* **2010**, *13*, 547–563. [CrossRef]
33. Gosecki, M.; Gadzinowski, M.; Gosecka, M.; Basinska, T.; Slomkowski, S. Polyglycidol, Its Derivatives, and Polyglycidol-Containing Copolymers—Synthesis and Medical Applications. *Polymers* **2016**, *8*, 227. [CrossRef]
34. Gadzinowski, M.; Kasprów, M.; Basinska, T.; Slomkowski, S.; Otulakowski, Ł.; Trzebicka, B.; Makowski, T. Synthesis, Hydrophilicity and Micellization of Coil-Brush Polystyrene-b-(Polyglycidol-g-Polyglycidol) Copolymer—Comparison with Linear Polystyrene-b-Polyglycidol. *Polymers* **2022**, *14*, 253. [CrossRef] [PubMed]
35. Otulakowski, Ł.; Kasprow, M.; Gadzinowski, M.; Slomkowski, S.; Makowski, T.; Basinska, T.; Forys, A.; Godzierz, M.; Trzebicka, B. Influence of Hydrophilic Block Length on the Aggregation Properties of Polyglycidol–Polystyrene–Polyglycidol Copolymers. *Soft Matter* **2024**, *20*, 546–557. [CrossRef]
36. Otulakowski, Ł.; Lipowska-Kur, D.; Gadzinowski, M.; Slomkowski, S.; Basinska, T.; Forys, A.; Trzebicka, B. The Synthesis and Properties of Brush-Coil–Brush (Polyglycidol-*g*-Polyglycidol)-*b*–Polystyrene–*b*-(Polyglycidol-*g*-Polyglycidol) Copolymers. *J. Phys. Chem. B* **2025**, *129*, 7406–7419. [CrossRef] [PubMed]
37. Vlassi, E.; Pispas, S. Imidazolium Quaternized Polymers Based On Poly(Chloromethyl Styrene) and Their Complexes with FBS Proteins and DNA. *Macromol. Chem. Phys.* **2015**, *216*, 1718–1728. [CrossRef]
38. Moad, G.; Rizzardo, E. Chapter 1. The History of Nitroxide-Mediated Polymerization. In *Nitroxide Mediated Polymerization: From Fundamentals to Applications in Materials Science*; Gigmes, D., Ed.; Polymer Chemistry Series; Royal Society of Chemistry: Cambridge, UK, 2015; pp. 1–44, ISBN 978-1-78262-061-7.
39. Greszta, D.; Matyjaszewski, K. Mechanism of Controlled/"Living" Radical Polymerization of Styrene in the Presence of Nitroxyl Radicals. Kinetics and Simulations. *Macromolecules* **1996**, *29*, 7661–7670. [CrossRef]
40. Namboodiri, V.V.; Varma, R.S. Solvent-Free Tetrahydropyranylation (THP) of Alcohols and Phenols and Their Regeneration by Catalytic Aluminum Chloride Hexahydrate. *Tetrahedron Lett.* **2002**, *43*, 1143–1146. [CrossRef]
41. Dimitrov, P.; Rangelov, S.; Dworak, A.; Haraguchi, N.; Hirao, A.; Tsvetanov, C.B. Triblock and Radial Star-Block Copolymers Comprised of Poly(Ethoxyethyl Glycidyl Ether), Polyglycidol, Poly(Propylene Oxide) and Polystyrene Obtained by Anionic Polymerization Initiated by Cs Initiators. *Macromol. Symp.* **2004**, *215*, 127–140. [CrossRef]
42. Mosmann, T. Rapid Colorimetric Assay for Cellular Growth and Survival: Application to Proliferation and Cytotoxicity Assays. *J. Immunol. Methods* **1983**, *65*, 55–63. [CrossRef]
43. Konstantinov, S.M.; Eibl, H.; Berger, M.R. BCR-ABL Influences the Antileukaemic Efficacy of Alkylphosphocholines. *Br. J. Haematol.* **1999**, *107*, 365–374. [CrossRef]
44. Taupin, P.; Zini, S.; Cesselin, F.; Ben-Ari, Y.; Roisin, M. Subcellular Fractionation on Percoll Gradient of Mossy Fiber Synaptosomes: Morphological and Biochemical Characterization in Control and Degranulated Rat Hippocampus. *J. Neurochem.* **1994**, *62*, 1586–1595. [CrossRef]
45. Mungarro-Menchaca, X.; Ferrera, P.; Morán, J.; Arias, C. β-Amyloid Peptide Induces Ultrastructural Changes in Synaptosomes and Potentiates Mitochondrial Dysfunction in the Presence of Ryanodine. *J. Neurosci. Res.* **2002**, *68*, 89–96. [CrossRef]
46. Robyt, J.F.; Ackerman, R.J.; Chittenden, C.G. Reaction of Protein Disulfide Groups with Ellman's Reagent: A Case Study of the Number of Sulfhydryl and Disulfide Groups in Aspergillus Oryzae α-Amylase, Papain, and Lysozyme. *Arch. Biochem. Biophys.* **1971**, *147*, 262–269. [CrossRef]
47. Shirani, M.; Alizadeh, S.; Mahdavinia, M.; Dehghani, M.A. The Ameliorative Effect of Quercetin on Bisphenol A-Induced Toxicity in Mitochondria Isolated from Rats. *Environ. Sci. Pollut. Res.* **2019**, *26*, 7688–7696. [CrossRef] [PubMed]

48. Ravindranath, V.; Anandatheerthavarada, H.K. Preparation of Brain Microsomes with Cytochrome P450 Activity Using Calcium Aggregation Method. *Anal. Biochem.* **1990**, *187*, 310–313. [CrossRef]
49. Mansuy, D.; Sassi, A.; Dansette, P.M.; Plat, M. A New Potent Inhibitor of Lipid Peroxidation In Vitro and In Vivo, the Hepatoprotective Drug Anisyldithiolthione. *Biochem. Biophys. Res. Commun.* **1986**, *135*, 1015–1021. [CrossRef] [PubMed]
50. *ISO 1110:1995*; Plastics—Polyamides—Accelerated Conditioning of Test Specimens. Technical Committee: ISO/TC 61/SC 9 Thermoplastic Materials. International Organization for Standardization: Geneva, Switzerland, 2019.
51. Shahrukh, M.; Ahmad, S.; Zaafar, M.; Hasan, N.; Ahmad, F.J. Management of Alzheimer's Disease With Nanotechnological Interventions and Novel Therapeutics. *Drug Dev. Res.* **2025**, *86*, e70120. [CrossRef] [PubMed]
52. Wang, D.; Chen, Z.; Wai Kan Yeung, A.; Atanasov, A.G. Differences between Common Endothelial Cell Models (Primary Human Aortic Endothelial Cells and EA.Hy926 Cells) Revealed through Transcriptomics, Bioinformatics, and Functional Analysis. *Curr. Res. Biotechnol.* **2021**, *3*, 135–145. [CrossRef]
53. Gangras, P.; Gelfanova, V.; Williams, G.D.; Handelman, S.K.; Smith, R.M.; Debets, M.F. Investigating SH-SY5Y Neuroblastoma Cell Surfaceome as a Model for Neuronal-Targeted Novel Therapeutic Modalities. *Int. J. Mol. Sci.* **2022**, *23*, 15062. [CrossRef]
54. *ISO 10993-5:2009*; Biological Evaluation of Medical Devices—Part 5: Tests for In Vitro Cytotoxicity. ICS 11.100.20. International Organization for Standardization: Geneva, Switzerland, 2017.